Tectonophysics 594 (2013) 38–59

Contents lists available at SciVerse ScienceDirect

Tectonophysics

journal homepage: www.elsevier.com/locate/tecto

SqueeSAR™ and GPS ground deformation monitoring of Santorini Volcano (1992–2012): Tectonic implications

E. Lagios [a,*], V. Sakkas [a], F. Novali [b], F. Bellotti [b], A. Ferretti [b], K. Vlachou [a], V. Dietrich [c]

[a] Remote Sensing Laboratory, Geophysics–Geothermics Dept., University of Athens, Panepistimiopolis-Ilissia, Athens 157 84, Greece
[b] Tele-Rilevamento Europa T.R.E. s.r.l., Ripa di Porta Ticinese 79, Milano 21149, Italy
[c] Institute for Geochemistry and Petrology, Swiss Federal Institute of Technology, CH-8092 Zurich, Switzerland

ARTICLE INFO

Article history:
Received 7 October 2012
Received in revised form 5 March 2013
Accepted 8 March 2013
Available online 18 March 2013

Keywords:
Santorini Volcano
Radar interferometry
PSInSAR
SqueeSAR
GPS measurements
Ground deformation

ABSTRACT

The Santorini Volcanic Complex (SVC) has been in a dormant state for the last 60 years until January 2011 when upward influx of magma reawakened the volcano with intense radial ground deformation and inter-caldera seismicity that lasted until January 2012 but declined afterwards. This paper aims to study the ground deformation and the inferred tectonic implications of the SVC for the period 1992–2012 mainly based on the SqueeSAR™ technique and DGPS campaign results of our local network which incorporates available data on Internet from several continuous GPS stations established on the island. The spatial deformation of the SVC during the *quiet* period 1992–2010 was deduced by joint analysis of ERS1 and 2 and ENVISAT. It was found that the intra caldera Palaea Kammeni shield volcano was being uplifted (2–3 mm/yr) with increasing rate, whilst the adjacent Nea Kammeni shield volcano was being subsided (up to 6 mm/yr) with increasing rate. The rest of the SVC showed a velocity field varying from −1 to +2 mm/yr, indicating a rather *linear* deformation during that period. The results from the GPS network are in full agreement with the SqueeSAR results. Based on the results of SqueeSAR analysis of 12 ENVISAT images, and DGPS/CGPS data to end 2012, the deformation for the unrest period 2011–2012 was *non-linear* being characterized by strong radial deformation in the northern part of the caldera (50–120 mm/yr), and accelerating values (>130 mm/yr^2). Combined GPS/SqueeSAR Mogi modeling indicated a source located north of Nea Kammeni at a shallow depth. However, a progressively decreasing rate in deformation was noted at most GPS/CGPS station components after January 2012, indicating magma settlement consistent with the constantly decreasing rate of the inter-caldera seismicity. The faulting features seem to have a key role in the evolution of the deformation, which continues up the end 2012, but at a very low level.

1. Introduction

The Santorini (Thera) Volcano is one of the most active in the Eastern Mediterranean area. A major Plinian eruption in the middle of the 17th century BC, causing a massive regional tsunami (Sigurdsson et al., 2006) and resultant destruction of the Minoan civilization, formed essentially the present caldera of the Santorini Volcanic Complex (SVC; Bond and Sparks, 1976; Dietrich, 2004; Druitt and Francaviglia, 1992; Druitt et al., 1989, 1999; Fytikas et al., 1984) which consists of Thera, Therassia, Aspronissi and the Kammenis (Palaea and Nea) Islets (Fig. 1). After that catastrophic episode, the volcano has been relatively quiet. The last significant eruption with lava outpour occurred in 1950 (Georgalas, 1953; Georgalas and Papastamatiou, 1953; Heiken and McCoy, 1984; Pyle and Elliott, 2006). Since early 1980, no significant ground deformation (which was of very small amplitude and only of a local character) has been observed or inferred on the basis of microgravimetric and EDM studies (Farmer et al., 2007; Lagios, 1995; Lagios et al., 1988, 1989; Stiros and Chassapis, 2003; Stiros et al., 2010).

No major seismic activity has also been observed in SVC since the early 1980's. Most of the micro-earthquake activity (Magnitudes (M) < 3) was rarely taking place inside the caldera, but to a large extent it was associated with the Columbo submarine shallow volcanic vent (Fig. 2a), about 10 km NE of Thera Island, and it was mostly of volcanic origin (e.g. Delibasis et al., 1995). However, in January 2011, a sudden unrest started taking place within the caldera and lasted up to February 2012 with the occurrence of a shallow seismic activity of earthquake magnitudes ranging between 1.0 < M < 3.2 (Chouliaras et al., 2012; Newman et al., 2012; Papadimitriou et al., 2012; Papazachos et al., 2012) and which was particularly felt by the local population of the island. At the same time, significant deformation rates exceeding 100 mm/yr in the northern part of the caldera were noticed and associated with magma influx which has been simulated as a Mogi source about 2 km north of Nea Kammeni and at a depth of less than 5 km (Newman et al., 2012).

After February 2012, there was a considerable decline in the seismicity rate inside the caldera, reaching almost negligible levels (Fig. 2b),

* Corresponding author. Tel.: +30 2107274424; fax: +30 2107274787.
E-mail address: lagios@geol.uoa.gr (E. Lagios).

0040-1951/$ – see front matter © 2013 Published by Elsevier B.V.
http://dx.doi.org/10.1016/j.tecto.2013.03.012

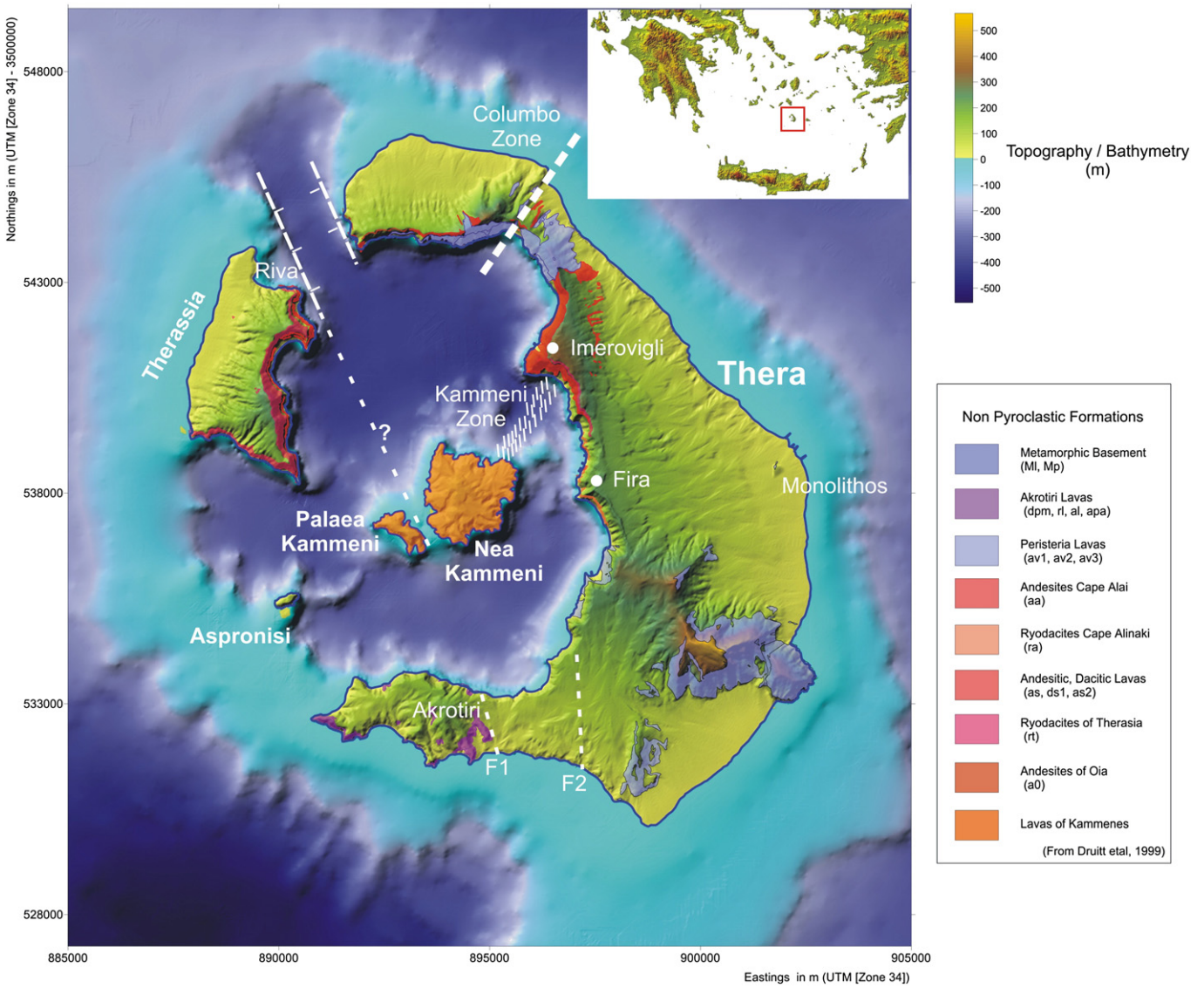

Fig. 1. The SVC showing some geological and major tectonic features (after Druitt et al., 1999). Faulting zones are discussed in the text. Bathymetry is after Nomikou et al. (2012a); UTM coordinates (Zone 34) in meters (Northing: Zone 34 — 3,500,000 m).

while a decrease in the amplitude deformation rates was observed at almost all GPS station components. Until the end of 2012, negligible seismicity inside the caldera was observed, while decreased ground deformation velocities were noted at the Differential GPS (DGPS) and Continuous GPS (CGPS) stations, including also a change in the velocity direction at some CGPS station components.

The purpose of the present paper is to (i) present a detailed spatial and temporal ground deformation of the SVC for the period 1992 to end 2012, outlining the importance of the *rate* (*increasing or decreasing*) of the velocity ground motion, (ii) demonstrate the role of the main geotectonic features on the resultant kinematics, involving also those inferred by geophysical interpretation, (iii) model the intense ground deformation during 2011–2012, and (iv) discuss the recent state of the Santorini Volcano.

The study of the ground deformation was based on (i) the detailed analysis of ERS and ENVISAT radar imaging, applying the SqueeSAR™ technique (an advanced methodology of the Permanent Scatterers (PS) SAR Interferometry — PSInSAR), (ii) the campaign results of DGPS analysis from remeasurements of our network (that was established in 1994) up to December 2012, and (iii) the available data from CGPS stations established in the SVC since 2006, which were later (2011) densed by various Institutions. The detailed outline of the ground deformation (1992–2012) is presented in two periods that is 1992 to 2010, during which the inter-caldera seismicity was insignificant – hereafter called *quiet* period – and 2011 to 2012, when the outbreak of the inter-caldera seismicity and the intense deformation took place — hereafter called *unrest* period.

2. Brief geotectonic setting

The SVC (Fig. 1), among other Quaternary volcanoes of the Aegean region (e.g. Fytikas et al., 1984), defines the Southern Aegean active volcanic arc in a continental environment of extensional tectonics (e.g. Floyd et al., 2010; Ganas and Parsons, 2009; Jackson, 1994). The extension was initiated in the area during Upper Miocene, changing subsequently direction from WNW–ESE to NE–SW, while currently is N–S to NW–SE (Mercier et al., 1989; Perissoratis, 1995). Detailed accounts of the caldera development during the Minoan eruption have been given by Heiken and McCoy (1984, 1990) and Druitt et al. (1999). The composite structure of the Santorini Caldera resulted from at least four collapsing events (Druitt and Francaviglia, 1992; Druitt et al., 1999, 2012). Recent volcanological and geochemical studies suggest the presence of different geochemically and mineralogically magmatic chambers beneath its caldera and the Columbo submarine volcano

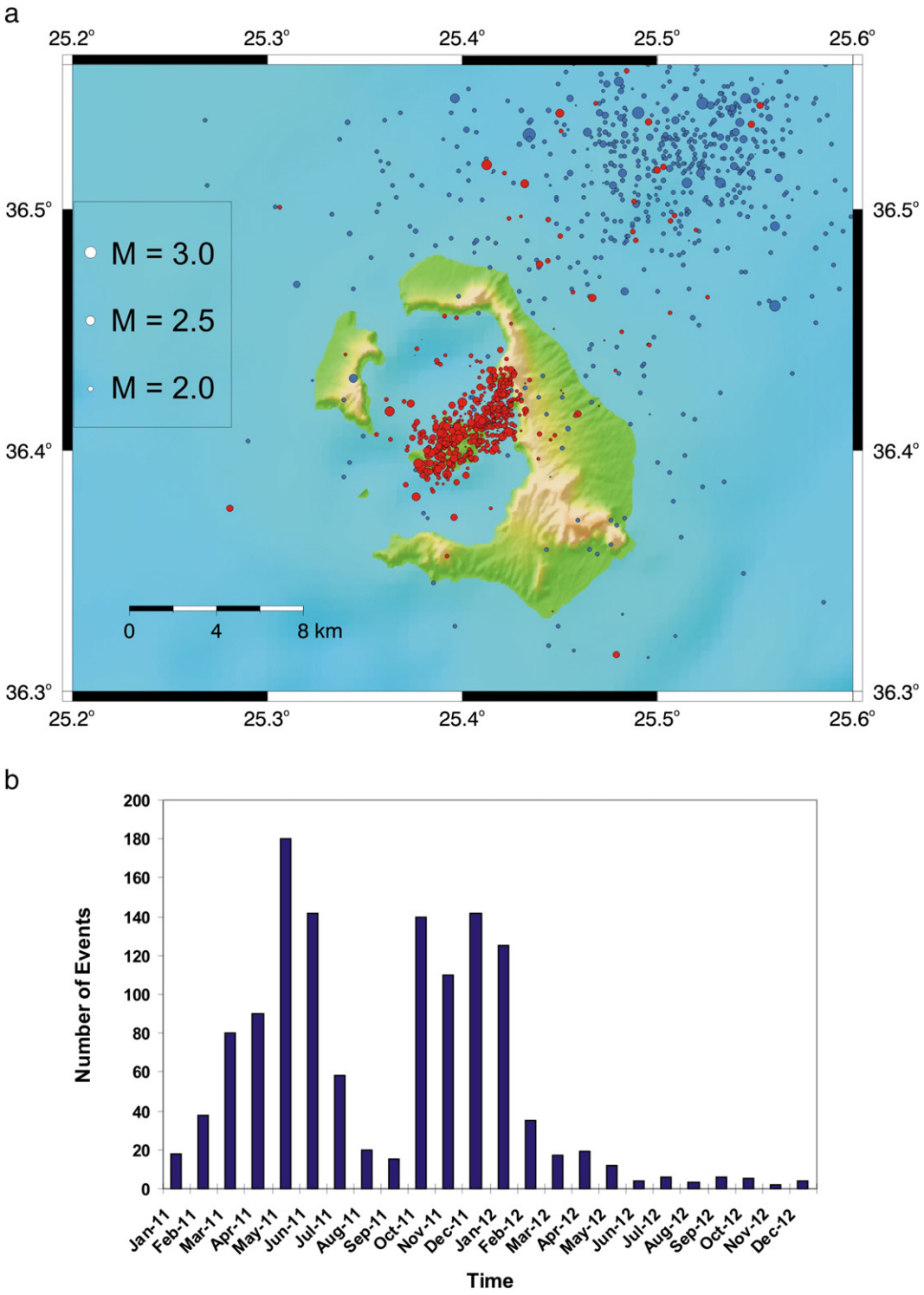

Fig. 2. (a) Earthquake epicenter distribution in the broader area of the SVC. Blue and red circles represent epicenters for the period 1990–2010 (after Papadimitriou et al., 2012), and 2011–2012 (National Observatory of Athens (NOA), Geodynamic Institute), respectively; (b) Histogram of monthly seismic events (M > 0.5) inside the Santorini Caldera for the period 2011–2012.

which is located a few kilometers offshore NE of Thera (Dimitriadis et al., 2009; Nomikou et al., 2012b; Sigurdsson et al., 2006). The latter could be an effect of depth of the different source regions of magma reservoirs, the Columbo chain being build up by magmas possibly derived directly from the mantle, whereas the Santorini Caldera forming magmas originated from intermediate crustal magma chambers and being contaminated significantly by partial crustal melting (Francalanci et al., 2005).

A low seismic velocity, tectono-volcanic fracture zone trending NE–SW of about 500 m width, called the *Kammenis Line/Zone*, is identified within the caldera (Fig. 1), along which most of the micro-earthquake activity has recently taking place (Fig. 2a). Another zone, almost parallel to the *Kammenis* one, is the *Columbo Faulting Zone* further to the north, which probably links the Kammenis volcanic center and the submarine volcano at Columbo (e.g. Nomikou et al., 2012b). Seismicity monitoring studies before 2010 (Bohnhoff et al.,

2004, 2006; Delibasis et al., 1995; Dimitriadis et al., 2009; Kolaitis, 2011) demonstrate that the activity was virtually limited within the Columbo area, but almost largely absent in the caldera. However, the recently outburst of micro-earthquake activity (Jan. 2011 to Feb. 2012), with magnitudes up to M = 3.2, was basically confined within the *Kammenis Zone* (Fig. 2a).

2.1. The gravity anomaly map

An important tectonic feature that plays a significant role in the general geodynamics and kinematics of the SVC is the Alpine basement and its subsurface extent, together with possible faults associated with it. The basement outcrops at the south-eastern part of Thera and to the Monolithos area where a small part of it emerges to the ground surface (Fig. 1). However, its accurate spatial extent is not well known since most of the southern part of Thera is covered by lavas (Druitt et al., 1999). A useful tool that may help clarifying the above issue is the gravity anomaly map (Fig. 3) compiled recently for the SVC (Chailas et al., 2012).

Considering this map, it may qualitatively be seen that the Alpine basement, outcropping at the southern part of Thera and extending to the Monolithos area to the north, is associated with the gravity high where the anomaly values are higher than about 130 mGal. Another interesting feature is the gravity low (110 mGal) identified around the Akrotiri area as due to the low density overburden (e.g. tuffs) and the partially met Akrotiri lavas. Additionally, two possible basement faults (F1 and F2, Fig. 3) running almost N–S have been interpreted at the southern part of Thera, marking a depression in the broader Akrotiri area, The Akrotiri Depression. The latter is in agreement with earlier Magnetotelluric analysis based on the induction vectors by Sotiropoulos et al. (1996) and updated by Papageorgiou et al. (2010). Another area of depression designated by a gravity low (<110 mGal) is the marine area extending between Thera and Therassia and to the north (Fig. 3) marking the Riva (Caldera) Depression (Fig. 1; Sakellariou et al., 2012). All the aforementioned tectonic features seem to play an important role, and help to explain the observed ground deformation and the kinematics of the area, as will be demonstrated further down.

3. Ground deformation: the *quiet* period (1992–2010)

3.1. The SqueeSAR™ technique

Conventional Synthetic Aperture Radar (SAR) Interferometry (InSAR) and Differential GPS (DGPS), together with tiltmeters, are widely used techniques to measure the ground deformation in volcanoes. However, techniques like tiltmeters and DGPS provide only point coverage, since they are detecting changes at single points (stations) on the ground surface. Spaceborne radar interferometry (Hanssen, 2001; Massonnet and Feigl, 1998) has already shown its

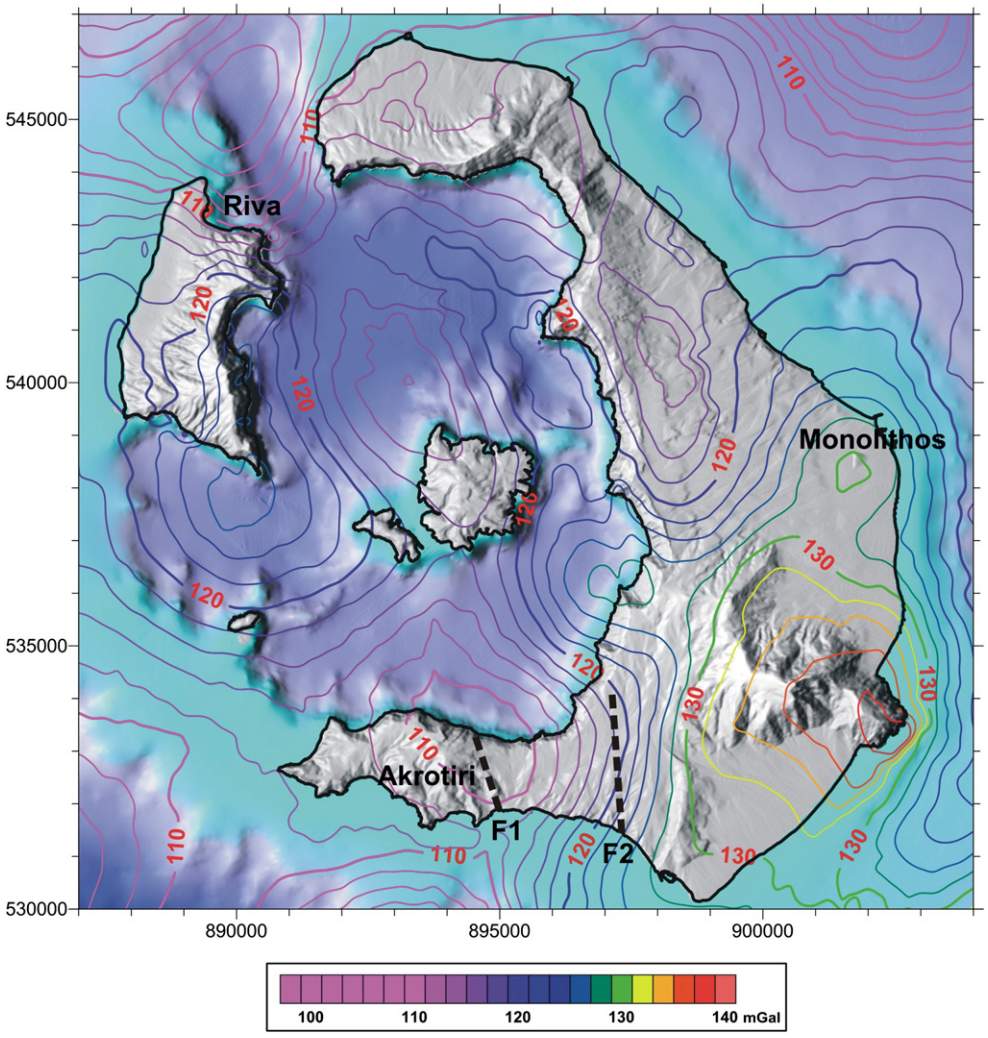

Fig. 3. Santorini gravity anomaly map referred to IGSN'71, GRF'67 and Bouguer density 2670 kg/m^3 (after Chailas et al., 2012); contour interval 2 mGal. Coordinates UTM (Zone 34) in meters (Northing: Zone 34 — 3,500,000 m).

ability in mapping ground deformation on a large spatial scale with short term data sampling rates, associated with either volcanoes (e.g. Amelung et al., 2000; Briole et al., 1997; Lagios et al., 2005a,b), co-seismic activity (e.g. Feng and Jónsson, 2012; Wen et al., 2012), or landslides (e.g. Cascini et al., 2010) etc. Conventional InSAR uses the phase difference between two SAR acquisitions to obtain the interferograms (Hanssen, 2001), but this processing technique has disadvantage issues relating to atmospheric noise that cannot be efficiently eliminated resulting to not entirely reliable interferograms that represent the ground deformation. This deficiency has been overcome by a specific analysis considering phase changes in a series of SAR images acquired at different times over the same region, producing a series of interferograms with respect to a "master" image, where small parts of the study area (pixels) exhibiting coherent phase behavior may be identified, the so-called *permanent scatterers* (PS), introducing thus the *PSInSAR*™ technique (Ferretti et al., 1999, 2000, 2001).

Therefore, the above analytical procedure involving multi-temporal radar acquisitions results in the calculation of time series of PS displacements, which show the actual motion of each PS along the satellite direction (line-of-sight (LOS)), now referred to as Persistent Scatterer Interferometry (PSI) (Kampes, 2006). Generally, PSI was widely adopted by the scientific community with applications on various fields such as volcanoes and active tectonics (e.g. Burgmann et al., 2006; Funning et al., 2007; Hooper et al., 2007; Lagios et al., 2011, 2012; Massironi et al., 2009; Peltier et al., 2010; Schmidt and

Table 1
SAR images used for SqueeSAR analysis (1992–2010).

Descending orbit, track: 150					Ascending orbit, track: 329				
id	Date	Satellite	Bn	Bt (days)	id	Date	Satellite	Bn	Bt (days)
1	16/06/1992	ERS-1	0.12	−2649	1	09/05/1993	ERS-1	−0.24	−1949
2	25/08/1992	ERS-1	0.22	−2579	2	13/06/1993	ERS-1	−0.42	−1914
3	29/09/1992	ERS-1	0.33	−2544	3	28/03/1995	ERS-1	−0.08	−1261
4	03/11/1992	ERS-1	0.77	−2509	4	07/03/1995	ERS-2	−0.18	−1190
5	08/12/1992	ERS-1	0.21	−2474	5	12/07/1995	ERS-2	0.05	−1155
6	23/03/1993	ERS-1	0.27	−2369	6	15/08/1995	ERS-1	0.03	−1121
7	27/04/1993	ERS-1	0.74	−2334	(M) 7	09/09/1998	ERS-2	0	0
8	06/07/1993	ERS-1	−0.56	−2264	8	18/11/1998	ERS-2	0.53	70
9	20/04/1995	ERS-1	0.06	−1611	9	23/12/1998	ERS-2	−0.24	105
10	26/05/1995	ERS-2	−0.05	−1575	10	27/01/1999	ERS-2	−0.09	140
11	29/06/1995	ERS-1	−0.68	−1541	11	16/06/1999	ERS-2	0.7	280
12	30/06/1995	ERS-2	−0.69	−1540	12	03/11/1999	ERS-2	0.03	420
13	07/09/1995	ERS-1	−0.75	−1471	13	31/05/2000	ERS-2	−0.85	630
14	08/09/1995	ERS-2	−0.8	−1470	14	20/02/2002	ERS-2	−0.26	1260
15	12/10/1995	ERS-1	0.66	−1436	15	12/03/2003	ENVS2-V	−0.27	1645
16	14/06/1996	ERS-2	−0.27	−1190	16	30/07/2003	ENVS2-V	−0.16	1785
17	23/08/1996	ERS-2	−0.48	−1120	17	03/09/2003	ENVS2-V	−0.24	1820
18	27/09/1996	ERS-2	−0.03	−1085	18	17/12/2003	ENVS2-V	0.46	1925
19	01/11/1996	ERS-2	0.99	−1050	19	25/02/2004	ENVS2-V	0.52	1995
20	15/05/1998	ERS-2	0.54	−490	20	31/03/2004	ENVS2-V	−0.15	2030
21	24/07/1998	ERS-2	−0.14	−420	21	14/07/2004	ENVS2-V	−0.06	2135
22	02/10/1998	ERS-2	0.67	−350	22	27/10/2004	ENVS2-V	−0.6	2240
23	11/12/1998	ERS-2	−0.71	−280	23	05/01/2005	ENVS2-V	0.61	2310
24	23/06/1999	ERS-2	−0.32	−175	24	25/05/2005	ENVS2-V	0.06	2450
25	30/04/1999	ERS-2	−0.15	−140	25	08/08/2007	ENVS2-V	0.19	3255
(M) 26	17/09/1999	ERS-2	0	0	26	18/06/2008	ENVS2-V	−0.03	3570
27	22/10/1999	ERS-2	−0.04	35	27	23/06/2010	ENVS2-V	0.19	4305
28	26/11/1999	ERS-2	0.07	70					
29	31/12/1999	ERS-2	0.54	105					
30	10/03/2000	ERS-2	0.01	175					
31	14/04/2000	ERS-2	0.18	210					
32	19/05/2000	ERS-2	0.29	245					
33	28/07/2000	ERS-2	−0.2	315					
34	10/11/2000	ERS-2	0.31	420					
35	15/12/2000	ERS-2	0.54	455					
36	09/05/2003	ENVS2-V	0.6	1330					
37	02/07/2004	ENVS2-V	−0.44	1750					
38	06/08/2004	ENVS2-V	0.06	1785					
39	10/09/2004	ENVS2-V	0.65	1820					
40	15/10/2004	ENVS2-V	0.43	1855					
41	24/12/2004	ENVS2-V	0.03	1925					
42	28/01/2005	ENVS2-V	0.01	1960					
43	08/04/2005	ENVS2-V	−0.07	2030					
44	13/05/2005	ENVS2-V	0.44	2065					
45	22/07/2005	ENVS2-V	0.51	2135					
46	26/08/2005	ENVS2-V	0.47	2170					
47	04/11/2005	ENVS2-V	0.52	2240					
48	17/02/2006	ENVS2-V	−0.13	1345					
49	24/03/2006	ENVS2-V	0.25	2380					
50	24/11/2006	ENVS2-V	−0.13	2625					
51	29/12/2006	ENVS2-V	0.35	2660					
52	26/02/2010	ENVS2-V	−0.2	3815					

M: master image.
Bn: critical normal baseline fraction (M) master image.
Bt: days elapsed from master image acquisition.

Burgmann, 2003; Werner et al., 2003; Zebker et al., 2007). However, PSInSAR™ was recently advanced and replaced by the SqueeSAR™ algorithm (Ferretti et al., 2011).

The SqueeSAR™ is a second generation of the PSI technique, searching targets from a radar imaging data-set that involve in its analysis not only identified consistent *p*ermanent *s*catterers (PS), but also homogeneous spatially *d*istributed *s*catterers (DS). PS usually correspond to man-made objects (e.g. buildings, linear structures, and open outcrops), while DS are typically identified by homogeneous ground surface, uncultivated, desert or debris covered areas, and scattered outcrops. All identified PS and DS are then jointly processed (taking into account their different statistical behavior) applying the PSInSAR algorithm. Because of the higher density of identified measurement points (scatterers), and their wider spatial coverage, millimeter accuracy on ground displacement values is achieved, together with reduced standard deviation values, compared to the previous PSInSAR™ algorithm (Ferretti et al., 2001). Therefore, an increased number of identified points on the ground results at an increased confidence of the ground motion, by identifying and "squeezing" all possible ground target information relating to acceptable coherent levels for estimated optimum phase values for the PSI analysis (Ferretti et al., 2011).

3.1.1. Application of SqueeSAR™ technique

Joint processing of 27 Ascending and 52 Descending orbital geometry SAR and ASAR scenes acquired by ERS-1 and 2 and ENVISAT satellites, respectively, was finally carried out, covering the period June 1992 to June 2010 (Table 1). More than 15,000 and 7000 PS/DS in descending (LOS angle 25.26°) and ascending (LOS angle 22.36°) geometry, respectively, were identified within an areal extent of about 80 km^2. Fig. 4 shows the SqueeSAR product of the LOS velocity deformation field (in mm/yr) for the *quiet* period.

The reference point that was chosen for the interferometric analysis is also shown in Fig. 4, and is located at the pre-volcanic island area (Heiken and McCoy, 1984) that constitutes the Alpine basement of Triassic Limestones (Druitt et al., 1999). The selected point assures the best quality for the processing of the radar imaging, presenting thus a low-noise time series and consequently resulting to a noise reduction of the data set. The point is located in the same geological unit and very close to the local reference station of our GPS network. As will be shown further down (Section 3.2), the area where our reference points (GPS and InSAR) are located is the most stable unit compared to the rest of the study area.

3.1.1.1. The velocity field. It is obvious that the SqueeSAR image of the ground velocity field from the ERS/ENVISAT descending data (Fig. 4a) has a significantly higher number of identified points as compared to the ascending one (Fig. 4b) because of the larger number of imaging acquisition. More emphasis, therefore, will be given to the descending product. Small LOS velocity values ranging from −2 to +2 mm/yr are observed on both images of the two largest islands (Thera and Therassia) of the SVC. However, a distinct differentiation is observed at the southern and northern part of Thera with predominantly negative LOS velocity values, indicating a motion away from the satellite in descending geometry, while positive LOS velocity values are evident in the ascending geometry (movement towards the satellite). The latter is a strong indication of a prominent E–W horizontal component. The rest of Thera Island (main central part) shows LOS velocity variation from −1 to +2 mm/yr.

The deformation study along the cliffs of the caldera is another major and effective contribution of the SqueeSAR technique. Due to the satellite orbital geometry associated with the ascending and descending acquisitions, the 18-year deformation along the cliffs at Therassia and Thera islands may be clearly "seen", respectively. Negative velocity values up to −1 mm/yr are mostly observed at Thera with an exception at the urban area of Fira, where positive velocity values (up to +2 mm/yr) are measured (Fig. 4a). In Therassia, positive velocity values are mainly observed (1–2 mm/yr), excluding its southern part where negative velocity values are noted (Fig. 4b).

Considering the deformation at the center of the SVC, Palaea and Nea Kammeni, the following issues may be outlined: (i) The same pattern of deformation is noticed on both ascending and descending products (Fig. 4), indicating a predominant vertical component of motion. (ii) A clear differentiation in the vertical pattern is evident between the two islets: Palaea Kammeni shows positive LOS velocity values of 3–5 mm/yr, indicating a continuous uplifting type of motion. However, Nea Kammeni shows positive velocity values at its northern part that gradually decrease towards the center and its southern part, reaching values smaller than −3 mm/yr, depicting a radial pattern of deformation.

The standard deviation of the velocity field was also computed both for the descending and ascending images (Fig. 5) presenting values quite smaller than 1 mm/yr, not only in the Thera and Therassia islands, but also in the Kammenis Islets. The standard deviation of velocity for the ascending data (Fig. 5b) appear to have higher values than the descending data (Fig. 5a), because of the significantly smaller number of radar imaging used for processing (Table 1). Two parameters are generally affecting the calculation of the standard deviation: (i) *The distance of each PS/DS point from the reference point.* In fact, the displacement model is estimated on the phase-difference between the point under analysis and the reference point, in order to mitigate the effect of the atmospheric noise, which is strongly spatially correlated. However, moving away from the reference point, the difference between its atmospheric contribution and the atmospheric contribution of the PS/DS point under analysis tends to increase producing a larger residual after the estimation of the linear model. The latter is represented by the standard deviation of the corresponding estimated average velocity. Therefore, the standard deviation of velocity increases moving away from the reference point. (ii) *The deviation of motion from the linear model.* Since the standard deviation is associated with the average rate of deformation, if a PS/DS point exhibits a strong non-linear motion then it would result in a large residual with respect to the linear model, and thus in a high standard deviation value. This, therefore, allows identifying areas being affected by motion-dynamics that are more complex than the linear model assumption, and in any case it shows a clear deviation from a linear velocity pattern of ground deformation.

Considering the above, it is inferred that generally an almost *linear* deformation is taking place in the SVC for the period 1992–2010. A small deviation from the above aspect may only be attributed at the Kammenis, where slightly higher standard deviation values are noticed, together with the half eastern part of Thera, and the half western part of Therassia.

3.1.1.2. The acceleration field. The acceleration field of the descending and ascending data is presented in Figs. 6 and 7, respectively. The acceleration field was obtained by fitting a second order polynomial to the time series of each PS/DS point. The acceleration field describes the rate of the velocity change of the PS/DS points; therefore the sign of the velocity (positive or negative) has to be taken into consideration. Considering PS/DS points with positive sign of velocity (i.e. uplift), positive acceleration is associated with an *increasing rate* of uplift, whereas a negative sign with a *decreasing rate*. For a negative sign of velocity (i.e. subsidence), positive acceleration is associated with a *decreasing rate* of subsidence, whereas a negative sign indicates an *increasing rate*. Note that the small computed values of acceleration (−0.4 to +0.4 mm/yr^2) – with an estimated standard deviation ranging from 1.1 to 3.2 mm/yr^2 – combined with the small values of standard deviation of velocity (<1 mm/yr) confirm the *linear* type of ground deformation in the study area. Nevertheless, it is worthy pointing out some aspects relating to the *deformation rate* which was taking place and associated with the *quiet* period (1992–2010).

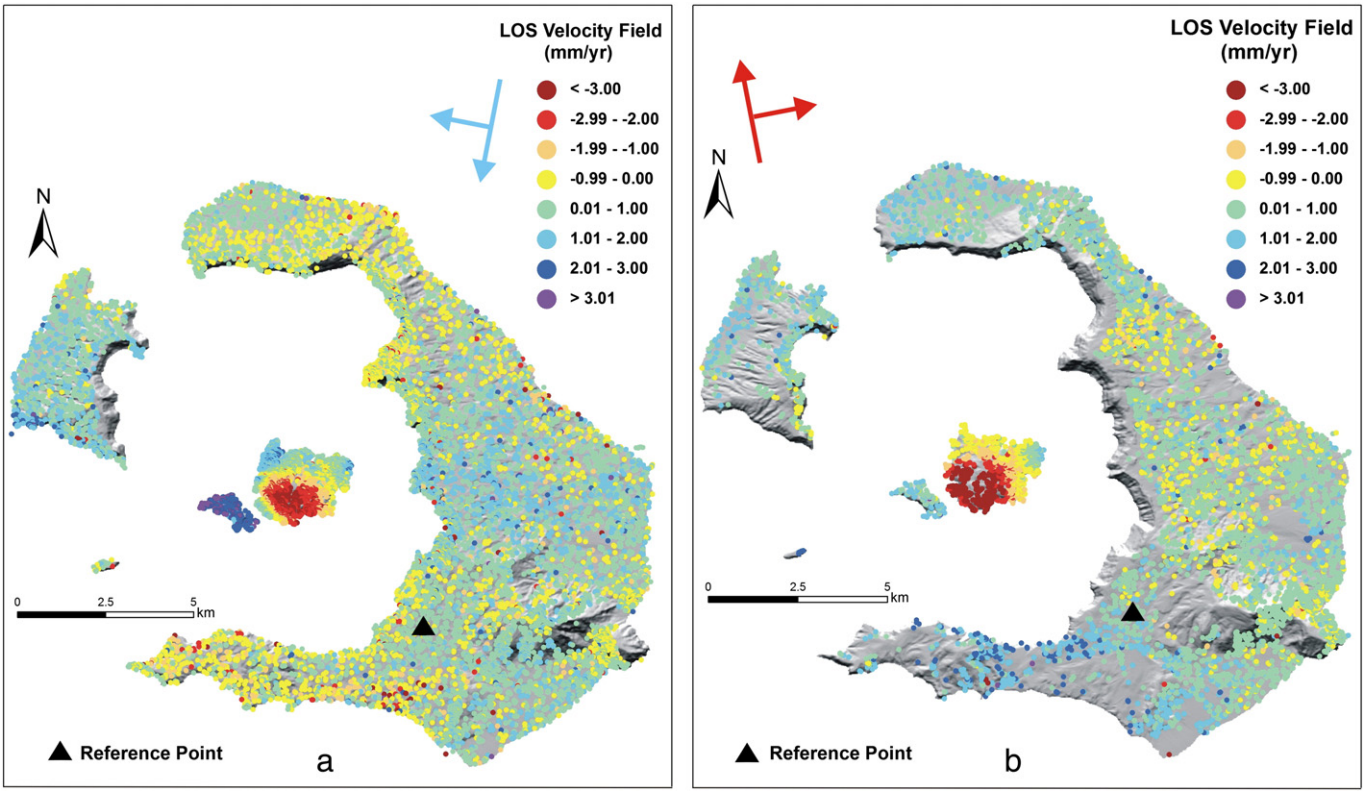

Fig. 4. LOS velocity ground maps (mm/yr) for (a) descending, and (b) ascending orbital satellite geometry deduced from a combined analysis of ERS and ENVISAT data for the period 1992–2010. Arrows indicate satellite orbital and acquisition geometry.

Negative velocity values, indicating ground motion away from the satellite (i.e. subsidence) were basically observed in the SW part of Thera characterized by a *decreasing rate* of motion, while *increasing rate* was noticed at its NE part, in the area across the Columbo Zone. The most significant negative velocity values though are observed in Nea Kammeni, where a *decreasing rate* of subsidence is evident from the descending data (Fig. 6a). However, when looking at the ascending data (Fig. 7a), an *increasing rate* of subsidence was peripherally noticed, while a *decreasing rate* was taking place at its center. Conclusively, the center of Nea Kammeni subsided slower than its margins.

Positive velocity values, indicating movement towards the satellite (i.e. uplift) are generally noticed almost everywhere in the SVC

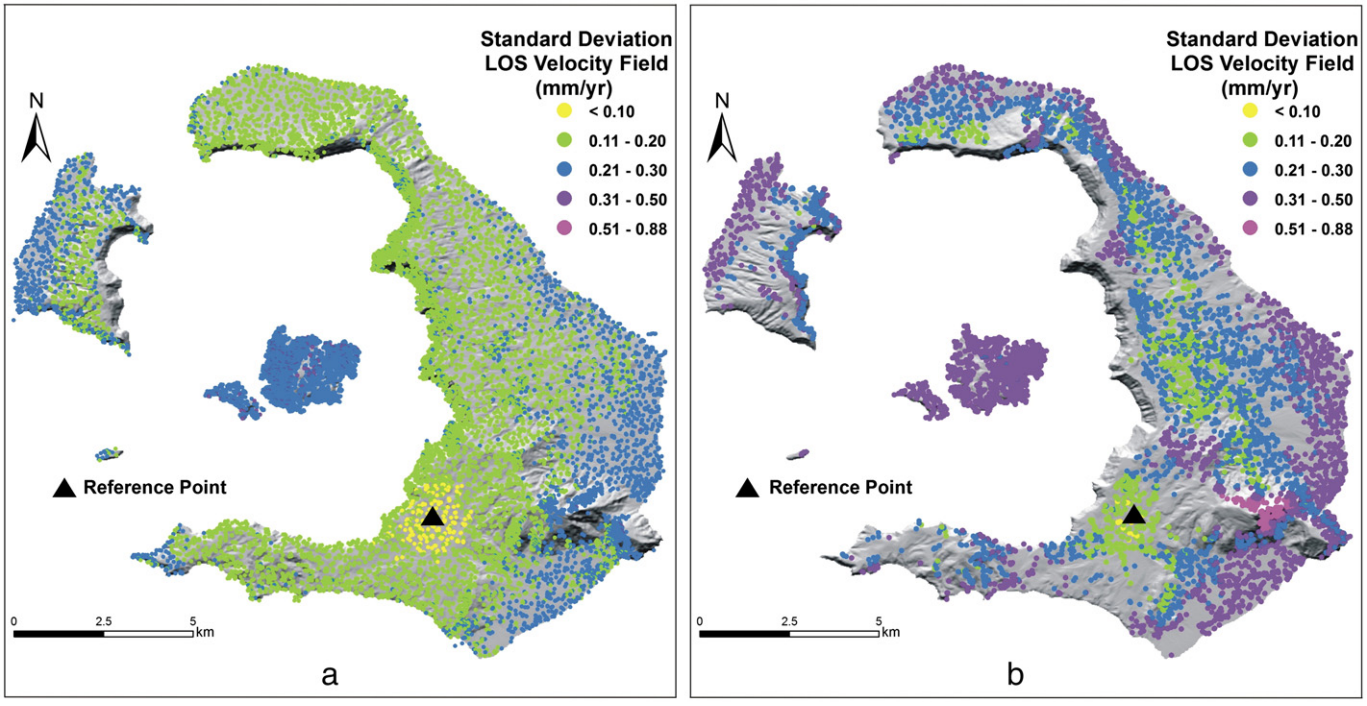

Fig. 5. Standard deviation of the LOS velocity field for (a) descending, and (b) ascending imaging acquisition (1992–2010).

(Figs. 6b and 7b), with the most evident areas the SE part of Thera, Palaea Kammeni and Therassia. Particularly, Palaea Kammeni is showing a predominantly *increasing rate* of uplift, while a *decreasing rate* of motion is observed in Therassia (Fig. 6b). Generally, a *decreasing rate* of motion is clearly exhibited at the SE part of Thera associated with the extent of the Alpine basement at this part of the island.

3.1.1.3. Vertical and east–west velocity components. The advantage of being able to process the ascending and descending radar images from the same area and overlapping period provides the possibility to calculate the *vertical* and *east–west* (E–W) velocity components of the deformation field. In order to estimate those components, the same targets are needed to be identified in both ascending and descending orbital geometry. Since this is almost impossible as the two geometries illuminate different objects, the ascending and descending data sets (Table 1) need to be resampled on the same 100 m × 100 m grid. Then the "common" cells of the created grid are used to calculate these velocity components. Analytical description of this procedure may be found in Bonforte et al. (2011). Considering the present data set of the SVC, about 2000 "common" points were identified applying this process, where the E–W and vertical components of the velocity field were extracted (Fig. 8).

Considering the Vertical Velocity component field (Fig. 8a), the most characteristic feature is the differential motion that Palaea and Nea Kammeni exhibit. Palaea Kammeni seems to have a consistent uplifted movement throughout the study period (1992–2010) with an average velocity of about +2 mm/yr. However, the adjacent Nea Kammeni seems to systematically subside. Only small fragments at the NE and NW parts of the islet are showing a moderate uplift. The rest gradually subsides towards the center, indicating thus a radial pattern of deformation (as also previously described — Fig. 7a): starting peripherally from +1 mm/yr, changing to moderate subsidence values of −1 to −2 mm/yr, reaching the highest values of subsidence at its center (−6 mm/yr). The vertical deformation in the rest of the islands does not show any specific pattern, with 'common' points of positive and negative velocity values irregularly distributed, ranging between −1 to +1 mm/yr.

Significant kinematic information may be extracted from the E–W velocity component field, where positive velocity values describe eastward motion, while negative values correspond to westward motion (Fig. 8b). The subsidence taking place in Nea Kammeni (Fig. 8a) has a strong influence in the E–W velocity component observed in the islet. Since the center strongly subsides, the eastern and western facing flanks of the islet have the tendency to 'collapse' toward its center, resulting thus to a westward and eastward horizontal motion, respectively. Palaea Kammeni although is systematically being uplifted, it also seems to have been affected by the subsiding Nea Kammeni, presenting thus an eastward motion, as the western flanks of Nea Kammeni.

In Thera Island, two prominent features arise: (i) The SW part that shows a strong westward motion (3–7 mm/yr), clearly being differentiated by the Alpine basement on the east (see fault mark in Fig. 1). (ii) The northern part west of the Columbo Zone that also shows a distinct westward motion.

A very limited number of common points identified in Therassia having mostly negative E–W velocity values indicate a westward motion of this island.

3.2. The Differential GPS measurements

The GPS network in SVC was first installed in 1994 (in cooperation with the University of Iceland, Freysteinn Sigmundsson) and remeasured several times up to December 2012 (Table 2). Generally, the stations were distributed on the islands and also on the Alpine basement. Several dual-frequency geodetic receivers (WILD type: SR299, SR399 and AX1200Pro, Trimble, Ashtech) were used in the GPS campaigns mounted on surveying tripods. The data were analyzed with the Bernese GPS software version 4.2 (Astronomical Institute, University of Berne, 2001) for campaigns until 2005, and version 5.0 (Dach et al., 2007) for the campaigns 2011 and 2012.

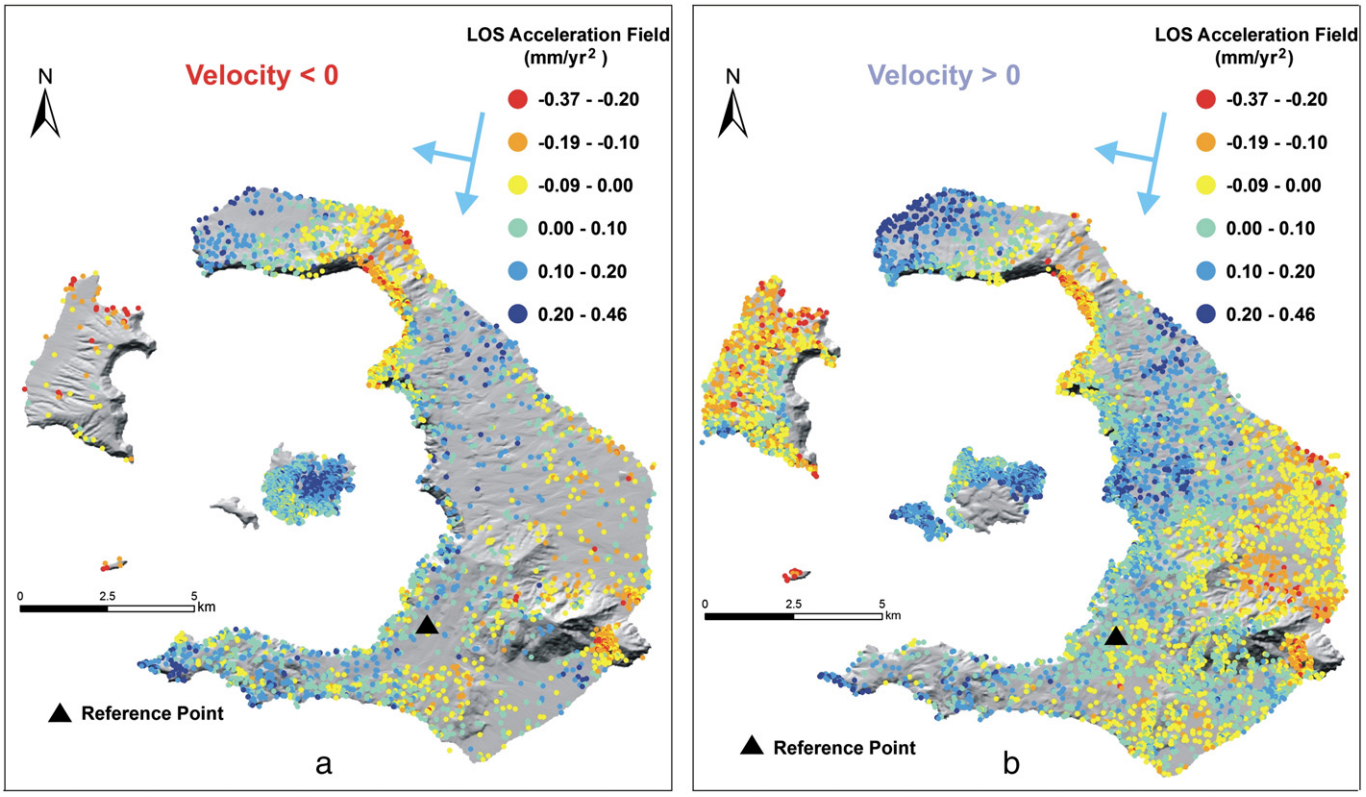

Fig. 6. Acceleration field of descending acquisition for (a) negative, and (b) positive LOS velocity values (1992–2010).

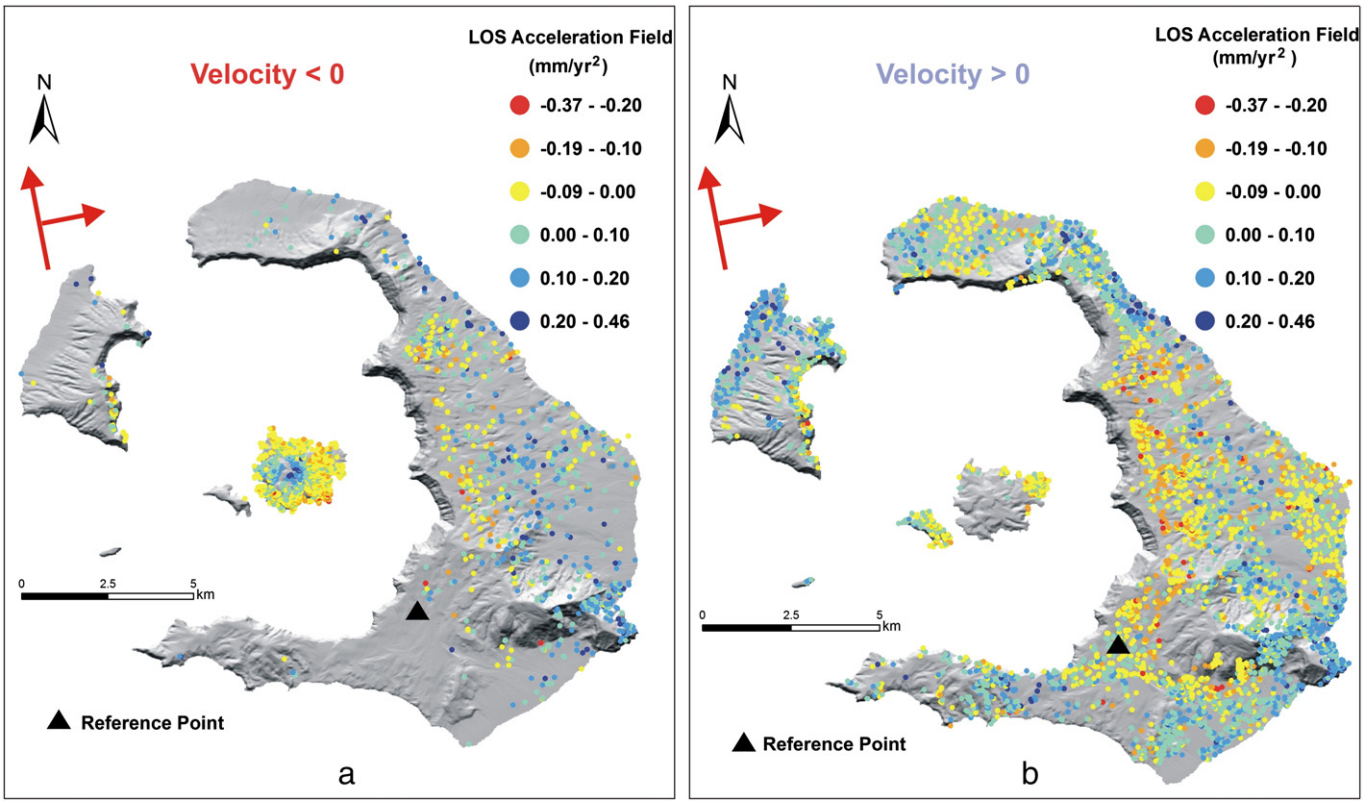

Fig. 7. Acceleration field of ascending acquisition for (a) negative, and (b) positive LOS velocity values (1992–2010).

Final IGS (International GNSS Service) products (e.g. satellite orbits and clocks) were used to calculate daily coordinates and troposphere parameters.

Each campaign was treated separately; the adopted procedure for the data acquisition was the same in all campaign periods. For each daily session, one station was selected as a "connecting station" in

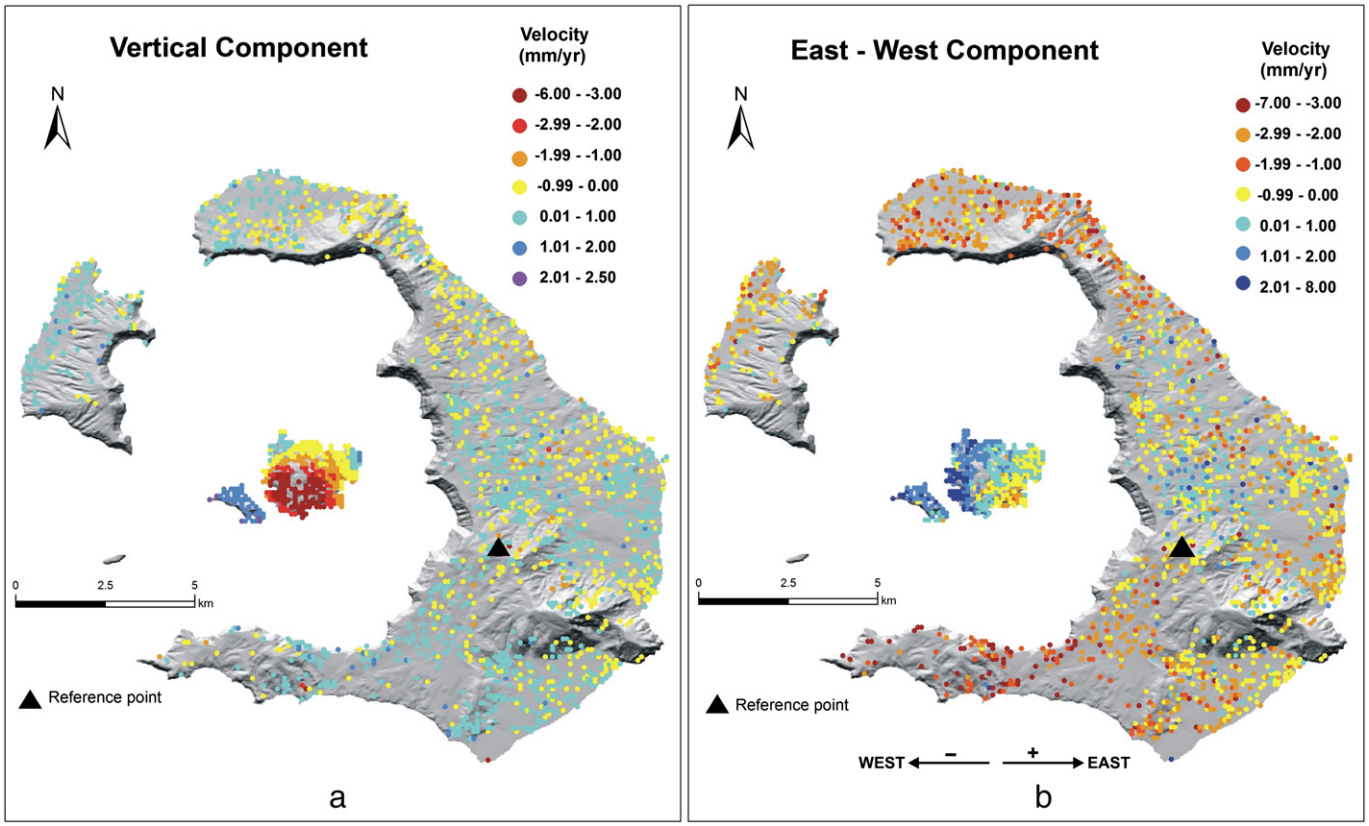

Fig. 8. Ground velocity maps of (a) the vertical, and (b) horizontal (in E–W direction) components deduced by combining ascending and descending data sets (1992–2010).

the center of the "roving" receiver stations and was tied to the local reference station no. 07. Each roving station was occupied at least twice with a recording time of at least 24 h (up to 92 h) and a sampling rate of 15 s. For each station, solutions for every daily session were computed and compared to its 'final' solution in order to evaluate the scatter of the coordinates deduced from each session. The final station coordinates for each campaign were obtained by combining the solutions of all daily sessions. Overall rms errors of about 1.0–5.3 mm and 2.0–8.1 mm for the horizontal and vertical components of displacement, respectively, were achieved for the majority of the stations (at a 90% confidence level).

Station no. 07 was chosen as local reference station, because of its location on the center of the Alpine basement in Thera and its anticipated better geological and tectonic stability compared to other parts of the complex. The station was operating continuously during all campaigns and tied to the ITRF2008 using the observational data from a number of IGS Reference Frame Stations in Europe (http://www.epncb.oma.be/), namely GRAZ (Graz, Austria), MATE (Matera, Italy), SOFI (Sofia, Bulgaria) and WTZR (Bad Kötzting, Germany) for the first remeasurement periods (up to 2005), and even more stations for 2011 and 2012, by introducing the coordinates and velocities with respect to ITRF2008. The analysis of the local reference station (no. 07) at earlier epochs was made using the Bernese v.4.2, while for the latest campaigns (2011–2012) it was performed using the Bernese Processing Engine (BPE), v.5.0.

The variation of the absolute coordinates for station no. 07 is presented in Fig. 9. This station has a horizontal motion to the SSE direction with respect to ITRF2008 ($V_{East} = 9.6 \pm 0.4$ mm/yr and $V_{North} = -18.1 \pm 0.3$ mm/yr), while the vertical component seems to be rather stable ($V_{Up} = 2.4 \pm 0.3$ mm/yr). The overall behavior of station no. 07 which is consistent with the anticipated regional motion (Hollenstein et al., 2008; Kahle et al., 1998) has to be particularly considered, since it represents the local reference point not only for the DGPS measurements, but also for the interferometric analysis. It is evident that the motion of this point seems to be rather constant not only during the *quiet* period up to 2010, but also during the *unrest* period 2011–2012.

3.2.1. The DGPS results

Calculation of velocity vectors with respect to ITRF2008 were made for all GPS stations for the period 1994–2005. A general motion to SSE (about 154° N) and amplitude of about 20 mm/yr was evident for all stations, describing basically the regional motion and hence obscuring the local, an order of magnitude lower-amplitude deformation velocity. Therefore, the local deformation is more clearly depicted when the GPS network is referred to the local reference station no. 07 (Fig. 10; Table 3). This velocity map could also represent the deformation field for the whole *quiet* period up to 2010. This is because, firstly, a *linear type of deformation* is deduced when considering the time-series of the GPS stations; secondly, the interferometric analysis has also pointed out that a *linear character* mostly defines the deformation for the *quiet* period 1992–2010 (Section 3.1.1).

Considering Fig. 10, the resultant velocity values are relatively small in both vertical and horizontal components ranging from −6 to +6 mm/yr and 0.5 to 3.5 mm/yr, respectively, and are similar to the ones determined by the interferometric processing (see Fig. 4). Most of the stations established along or close to the rim of the caldera on Thera have horizontal velocity vectors that point inwards. There is an exception though at the southern and northern part of Thera, where a westward component is clearly observed, particularly west of the Columbo Zone on the north, and to a lesser extent west of the Alpine basement on the south. The latter characteristic is consistent with the results of the E–W component shown by the SqueeSAR analysis (Fig. 8b). At the same time, the vertical velocity component at Thera varies from −2 to +3 mm/yr with some local exceptions at a couple of stations (no. 18 and no. 27).

Table 2
Occupied stations during GPS campaigns in Santorini Volcanic Complex.

GPS station no.	June 1994	Oct. 1995	July 1996	July 1998	Aug. 2005	Sept. 2011	June 2012	Sept. 2012	Dec. 2012
02	√	√	–	√	√	√	√	√	√
04	√	√	–	√	√	√	√	√	√
05	√	√	–	√	–	√	√	√	√
06	√	√	–	√	√	√	√	√	√
07	√	√	√	√	√	√	√	√	√
10	√	√	–	–	–	–	–	–	–
12	√	–	–	–	√	√	√	√	–
14	√	√	–	√	√	–	–	–	–
15	√	√	–	–	√	√	√	√	√
18	√	√	–	–	√	√	√	√	√
22	√	√	√	–	√	√	√	√	√
26	√	√	–	–	√	√	√	√	√
27	√	√	–	√	√	√	√	√	√
29	√	√	–	√	√	√	√	√	√
30	√	√	–	–	–	–	–	–	–
33	√	√	√	√	√	√	√	√	√
43	√	√	–	√	√	√	√	√	√
45	√	√	–	√	√	√	√	√	√
55	–	–	–	–	–	–	√	√	√
56	√	√	√	√	√	√	√	√	√
57	√	–	–	–	√	√	√	√	√
88	–	–	–	–	–	–	√	√	√
99	√	√	–	–	√	√	√	√	√

The observed GPS vertical deformation at the four stations on Nea Kammeni (−1 to −6 mm/yr) shows a gradual deformation pattern, where the stations located closer to the center exhibit larger values of subsidence. The latter is in good agreement with the identified InSAR vertical velocity field already discussed above (Fig. 8a), and earlier results of conventional Differential InSAR processing (Lagios et al., 2005a). The horizontal velocity vectors of these stations pointing at SW direction are compatible with the expected horizontal motion component of the subsiding islet collapsing at its center with higher rates. Finally note that Therassia migrates towards NW with small horizontal velocity values (1.5–2.0 mm/yr) compatible with the westward component outlined by the present interferometric analysis (Fig. 8b), and previous work by Stiros et al. (2010).

4. Ground deformation: the *unrest* period (2011–2012)

4.1. The SqueeSAR™ data analysis

Processing of 12 descending ASAR scenes acquired almost every month by ENVISAT satellite was carried out, covering the period April 2011 to March 2012 (Table 4). About 12,000 PS/DS points were identified within an areal extent of about 80 km^2 (Fig. 11). The LOS angle for this data set (that is about 39°) is noticeably larger than the one used for the period 1992–2010. That increased value of LOS angle has an immediate impact on the versor coordinates of the LOS deformation vector. Analytically, the E–W and vertical components are now 0.62 and 0.78, compared to 0.42 and 0.93 of Table 1 data set, respectively, while the N–S component is very small (−0.12, positive to north). That is a strong horizontal component is now inherent in the LOS direction of the ground deformation of the area, and this issue has to be taken into consideration when interpreting the data. A great help to interpret this ground deformation image will be provided by the DGPS observations. The reference point that was chosen for the interferometric analysis is also shown in Fig. 11, at a very close distance to the GPS network reference point; it is located at the Alpine basement, where no significant change of ground motion seems to have taken place even throughout of the *unrest* period (see Fig. 9).

Strong ground deformation of even two orders of magnitude (up to 110 mm/yr) is now obvious as taking place (Fig. 11) compared to the previous *quiet* period (Fig. 4). *Non-linear type of deformation* is

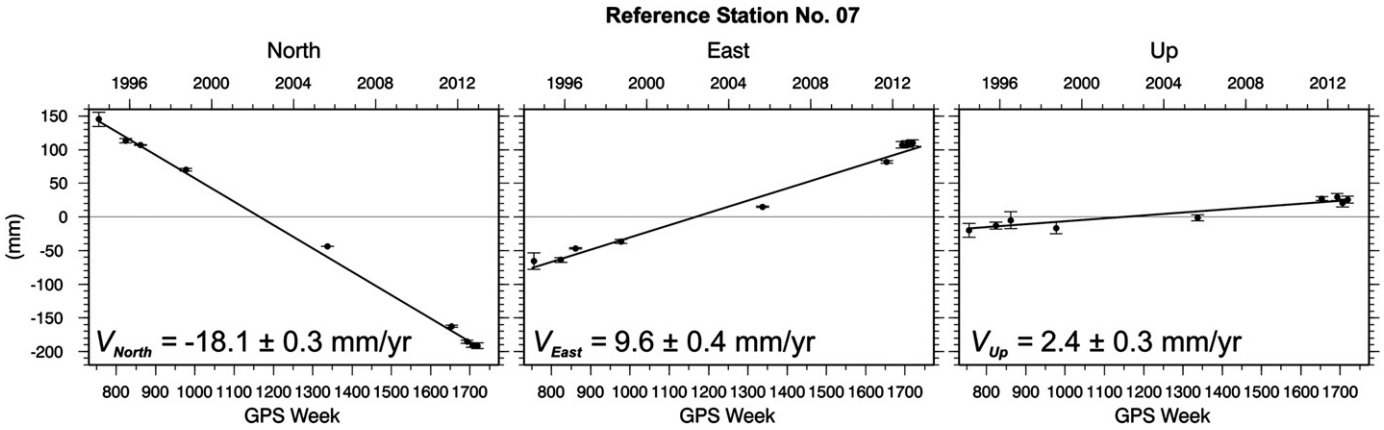

Fig. 9. Component displacements of the no. 07 GPS reference station with respect to ITRF2008 for the period 1994–2012.

also confirmed considering (i) the high standard deviation values (>6 mm/yr) of the LOS velocity field (Fig. 11b), and (ii) the very high values (up to 150 mm/yr^2) of the acceleration field (Fig. 12).

4.1.1. The velocity field

The high positive deformation values in the northern caldera presented a pattern of almost radial character (Fig. 11a), showing ground motion toward the satellite. A gradual radial decrease of the LOS velocity field was clearly depicted at the northern part of Thera, where high values were observed in the northern part of Nea Kammeni and some parts of the western Thera rims (>60 mm/yr) (Imerovigli area) that gradually decrease to negative values on the East. A significant change of the deformation pattern was observed across the Columbo Zone, marking the important role of this feature in the local kinematics. The smaller deformation values west of the Columbo Zone should be attributed to a strong northward component of motion in the northern part of Thera that cannot be depicted by the interferometric technique in the N–S direction. In a similar way, Therassia showed small positive (about +10 mm/yr) and mainly negative LOS velocity values (about −10 mm/yr), representing motion away from the satellite, consistent with a significant westward horizontal component, confirming thus the radial

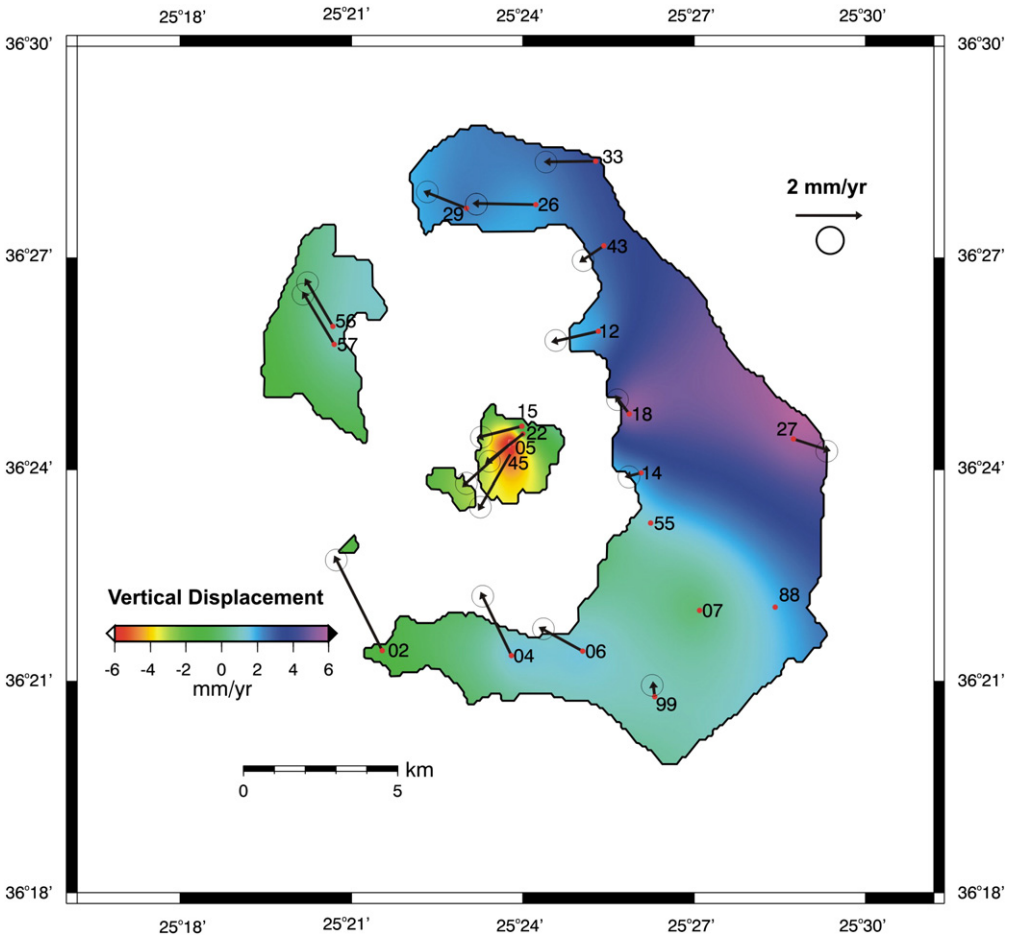

Fig. 10. GPS ground velocity map (mm/yr) for the *quiet* period 1994–2005.

Table 3
GPS velocity and amplitude deformation fields of Santorini Volcanic Complex.

GPS station	GPS velocity field: 1994–2005 Referred to no. 07						Deformation field: Sept. 2011–June 2012 Referred to ITRF 2008					
	V_{East} (mm/yr)	σV_{East} (mm/yr)	V_{North} (mm/yr)	σV_{North} (mm/yr)	V_{Up} (mm/yr)	σV_{Up} (mm/yr)	E–W (mm)	σ_{E-W} (mm)	N–S (mm)	σ_{N-S} (mm)	Up (mm)	σ_{Up} (mm)
02	−1.47	0.55	2.93	0.51	−1.08	1.00	−3.4	3.1	−29.1	3.5	20.1	7.9
04	−0.94	0.71	1.95	0.52	1.52	0.61	3.8	3.2	−27.7	3.7	5.5	7.4
05	−1.50	0.51	−1.35	0.76	−6.46	0.53	17.2	4.1	−46.2	5.3	54.5	7.1
06	−1.32	0.78	0.73	0.81	1.51	0.71	12.2	2.9	−26.4	3.2	5.2	6.4
07	–	–	–	–	–	–	25.2	0.9	−23.0	1.1	2.6	1.5
12	−1.43	–	−0.33	–	2.01	–	64.5	3.1	7.1	4.3	53.1	7.9
14	−0.46	0.62	−0.12	0.62	2.11	1.12	–	–	–	–	–	–
15	−1.37	0.61	−0.35	0.89	−0.73	0.51	23.1	2.3	−47.8	2.9	65.1	6.5
18	−0.41	0.82	0.55	1.10	5.75	1.61	47.2	1.7	−20.8	1.8	36.6	4.2
22	−1.14	0.71	−0.91	0.82	−1.69	1.10	19.0	2.8	−49.5	3.5	61.4	7.2
26	−1.93	0.62	0.04	0.71	2.03	1.01	17.8	2.5	41.3	3.0	25.2	6.8
27	1.11	0.85	−0.36	0.95	5.83	1.10	28.5	1.8	−18.0	2.1	12.6	4.8
29	−1.30	0.52	0.52	0.81	2.49	0.80	0.3	1.0	41.6	1.3	44.2	2.8
33	−1.57	0.64	−0.02	0.98	3.38	0.75	22.0	1.8	16.8	2.0	22.7	4.7
43	−0.72	0.54	−0.49	0.81	3.00	0.50	38.8	1.7	19.9	2.0	33.9	4.4
45	−1.01	0.57	−1.78	0.75	−5.48	1.05	15.1	2.6	−51.1	3.2	46.4	6.4
56	−0.84	0.51	1.45	0.85	0.88	0.46	−48.4	2.0	−0.7	2.5	40.9	5.7
57	−0.96	–	1.61	–	0.86	–	−51.7	1.8	−4.7	2.2	44.8	4.9
99	−0.05	0.81	0.43	0.84	1.02	0.56	19.8	2.9	−16.4	3.4	4.9	6.6
SANT	–	–	–	–	–	–	57.2	1.5	9.4	0.9	52.6	2.1
NOMI	–	–	–	–	–	–	50.9	0.9	−8.5	0.6	47.2	1.8
MOZI	–	–	–	–	–	–	38.9	2.4	25.1	1.8	38.3	4.8
RIBA	–	–	–	–	–	–	−33.2	1.5	15.4	1.3	25.2	4.6
KERA	–	–	–	–	–	–	−49	1.5	−15.2	0.9	41.4	2.6
PKMN	–	–	–	–	–	–	−2.6	0.9	−49.4	1.2	40.3	3.1

GPS station	Deformation field: June–Sept. 2012 Referred to ITRF 2008						Deformation field: Sept.–Dec. 2012 Referred to ITRF 2008					
	E–W (mm)	σ_{E-W} (mm)	N–S (mm)	σ_{N-S} (mm)	Up (mm)	σ_{Up} (mm)	E–W (mm)	σ_{E-W} (mm)	N–S (mm)	σ_{N-S} (mm)	Up (mm)	σ_{Up} (mm)
02	−0.82	2.46	−11.51	2.82	−3.10	6.31	7.10	2.64	−1.60	3.00	−3.40	6.78
04	3.30	2.34	−9.30	2.77	8.30	6.17	4.70	2.92	−0.60	3.41	−4.81	7.63
05	2.10	3.28	−8.60	3.86	0.90	8.27	−0.50	2.14	−1.70	2.50	−9.90	5.50
06	4.00	2.41	−11.40	2.69	9.60	6.16	−2.80	2.26	−2.30	2.62	−7.80	5.87
07	1.10	1.41	−4.80	1.41	−9.09	1.41	1.90	1.41	−1.10	1.41	4.97	1.41
12	2.00	3.50	−4.73	4.69	−3.01	8.70	–	–	–	–	–	–
15	5.80	1.86	−9.30	2.22	−12.20	4.80	−2.80	1.98	−0.20	2.34	−7.80	5.17
18	−1.60	1.41	−5.20	1.56	6.10	3.54	4.14	2.79	−0.73	3.20	−4.50	7.15
22	8.80	2.88	−8.50	3.41	−1.20	7.13	−3.80	2.33	−0.50	2.62	−13.10	5.87
26	1.70	1.84	−5.50	2.05	−3.39	4.61	2.70	2.00	−0.40	2.28	9.61	5.00
27	3.20	1.36	−3.20	1.64	2.60	3.72	1.00	3.49	0.40	4.03	−5.70	8.97
29	1.00	0.85	−1.50	0.99	1.10	2.12	2.60	1.25	−0.70	1.39	−3.49	3.09
33	0.10	1.75	3.20	2.02	11.60	4.58	−2.20	2.85	−1.80	3.29	−3.40	7.31
43	0.65	1.06	−1.93	1.20	−1.40	2.62	2.70	1.75	−4.60	2.06	6.90	4.53
45	2.10	1.84	−6.80	2.13	−12.00	4.74	0.80	1.91	−1.00	2.19	−0.20	4.81
55	−0.50	2.20	−8.80	2.48	−6.59	5.61	−1.50	2.46	1.70	2.82	3.39	6.26
56	−2.10	2.24	−4.70	2.59	1.60	5.46	2.89	3.25	−2.43	3.69	−1.10	8.13
57	0.20	1.61	−6.50	1.75	5.00	4.08	1.80	2.92	−2.50	3.28	6.10	7.40
88	−0.60	2.02	−4.40	2.39	−9.31	5.41	−2.70	2.20	2.50	2.48	6.50	5.69
99	−0.39	2.36	−11.40	2.72	5.29	6.14	−1.80	2.27	−2.50	2.62	−1.00	5.89
SANT	2.70	1.10	−6.10	1.10	−0.49	2.41	0.20	1.21	−1.40	1.31	6.10	2.60
NOMI	3.00	1.10	−6.50	1.10	0.70	2.41	1.50	1.32	−0.70	1.23	7.69	2.51
MOZI	2.50	0.95	−4.70	1.10	−1.28	2.35	−0.20	1.51	−0.30	1.35	7.39	2.35
RIBA	1.30	0.90	−6.30	1.01	0.80	2.50	0.00	1.41	0.60	1.38	2.10	2.51
KERA	−0.40	1.10	−5.20	1.10	−1.21	2.31	0.80	1.18	−0.30	1.64	4.10	2.46
PKMN	0.90	0.90	−7.80	1.21	0.31	2.20	0.30	1.25	−0.10	1.71	4.00	1.98
MKMN	2.30	1.41	−6.80	1.35	−0.31	3.20	–	–	–	–	–	–

σ: velocity and amplitude errors.

character of the observed ground deformation in the northern part of the caldera.

Negative LOS velocity values (motion away from the satellite) were observed in the E-SE part of Thera, an area that may be attributed to the underlined Alpine basement (Heiken and McCoy, 1984) extending also to Monolithos area, as has been inferred from the gravity anomaly map (Fig. 3). However, when adding the projected velocity vector of the common GPS/InSAR reference station (Fig. 9) on the LOS direction (10.5 mm/yr LOS) then the above area adjusts close to zero level, indicating stability. Finally, it appears that the radial deformation observed in the northern part of the caldera does not exist in the southern part, where the two inferred faults (F1 and F2) are forming the Akrotiri depression. These two faults differentiated the deformation pattern across them (Fig. 11c).

4.1.2. The acceleration field

High acceleration values (standard deviation ranging from 1.2 to 2.5 mm/yr^2) reaching locally more than 150 mm/yr^2 were mainly

computed for positive LOS velocity values in the Kammenis, and about 70 mm/yr^2 along the northern caldera cliffs (Fig. 12a). However, moving towards the eastern and southern parts of Thera, the acceleration values were significantly lower (about 20–30 mm/yr^2), reaching also negative values and showing that the deformation rate was smaller moving away from the northern caldera part. In the southern part of Thera, in the depression zone of Akrotiri area, negative acceleration values were observed marking in a more evident manner (compared to the LOS velocity field) the depression zone in this area. The acceleration field for negative velocity values (Fig. 12b) was rather limited, appearing only at some parts of Therassia and areas associated with the Alpine basement, indicating increasing rate of motion away from satellite. The moderate negative acceleration values in Therassia (about −35 mm/yr^2) showed an increasing rate of motion away from satellite (westward motion).

4.1.3. The Kammenis Islets

The most substantial deformation was taking place in Palaea and Nea Kammeni where the largest positive velocity and acceleration values were observed (Fig. 13), meaning that an increasing rate of motion has taken place towards the satellite (basically uplift). The strong *non-linear* character of deformation was evident by the highest standard deviation (Fig. 11b) and acceleration values (Fig. 13b). The LOS velocity field for these two islets (Fig. 13a) showed a clear gradient pattern, with decreasing velocity values from north to south. The highest velocity values were observed in the northern coast of Nea Kammeni (up to almost 90 mm/yr), decreasing to about 30 mm/yr in Palaea Kammeni. However, when considering the acceleration field (Fig. 13b), Palaea Kammeni and the southwestern part of Nea Kammeni have exhibited the highest positive acceleration values (up to 210 mm/yr^2), signifying the intense rate of deformation in this part. The southeastern part of Nea Kammeni that is associated with the latest lava effusions, as having the lowest (positive) acceleration values, seemed to have been moved with the lowest rate compared to the other parts of the two Kammenis.

4.2. The GPS measurements

Four campaigns were made within the *unrest* period that is in Sept. 2011, June, Sept. and Dec. 2012 (Table 2). The ground deformation amplitude differences are shown in Table 3. A Continuous GPS (CGPS) station recording at 1 Hz frequency was established in Imerovigli (Thera) by the Geophysics Department of the University of Athens (NKUA) in July 2011. That station (named SANT) recording both GPS and GLONASS satellite systems (GNSS) was an additional one to the already CGPS existing and operating stations (NOMI, MOZI, RIBA, KERA, PKMN, and MKMN) in the SVC by the Georgia Institute of Technology (USA) and University of Patras (GR), their data of which are provided by the UNAVCO Organization (www.unavco.org). Processing of all available to us data is performed on a daily basis using the BPE.

Table 4
ASAR images used for SqueeSAR analysis (2011–2012).

id	Date	Satellite	Bn	Bt (days)
1	02/04/2011	ENVS6-V	0.04	−180
2	02/05/2011	ENVS6-V	0.01	−150
3	01/07/2011	ENVS6-V	0.04	−90
4	31/07/2011	ENVS6-V	0.00	−60
5	30/08/2011	ENVS6-V	0.06	−30
(M) 6	29/09/2011	ENVS6-V	0	0
7	29/10/2011	ENVS6-V	−0.07	30
8	28/11/2011	ENVS6-V	−0.04	60
9	28/12/2011	ENVS6-V	−0.04	90
10	27/01/2012	ENVS6-V	−0.01	120
11	26/02/2012	ENVS6-V	0.05	150
12	27/03/2012	ENVS6-V	0.07	180

M: master image.
Bn: critical normal baseline fraction (M) master image.
Bt: days elapsed from master image acquisition.

4.2.1. Period September 2011–June 2012

The GPS results that include both campaign and CGPS/GNSS data are presented in Fig. 14 and referred to the local reference station no. 07 (Fig. 14a), and to ITRF2008 (Fig. 14b). A strong radial ground deformation is evident particularly at the northern part of the caldera with amplitudes ranging from 30 to 60 mm, while the uplift is up to 30–65 mm, being consistent with previously published work (Newman et al., 2012).

In the southern part of the caldera, the horizontal GPS displacement vectors are of much smaller values (up to 29 mm), showing also a differentiation from the radial pattern observed in the northern part of the caldera. Displacement vectors ranging from 12 to 29 mm are noticed pointing SW in the southern part of Thera, together with the broader area underlied by the Alpine basement where the motion is to SE, demonstrating the regional motion with respect to ITRF2008. The strain field was calculated based on the GPS displacement vectors (Pesci and Teza, 2007) from these two period campaigns (Fig. 14c). The clear extensional pattern observed in both axes of the strain field is very clear in the northern part of the caldera.

4.2.2. Period June–September 2012

For the next GPS remeasurement period June to Sept. 2012 (Fig. 15a), the overall image of the ground deformation is significantly different from the previous one. Small displacement amplitudes that do not exceed 12 mm were observed in both horizontal and vertical components at almost all of the stations. The radial pattern of deformation that was prevailing previously does not exist anymore in the northern part of the caldera. The deformation amplitudes have been reduced at the Kammenis by an order of magnitude. The horizontal vectors have been rotated to an almost SSE direction. In south Thera, the deformation seems to preserve the previous pattern of motion but with decreased amplitudes.

4.2.3. Period September–December 2012

During the last campaign period Sept. to Dec. 2012 (Fig. 15b), the observed amplitudes of deformation vectors have been further decreased reaching values just above their error estimates. There are though two patterns to point out. One at the NE part of Thera across the Columbo Line where a slight uplift (about 8–10 mm) is observed, and another one at Nea Kammeni where a slight subsidence (about 8 mm) is taking place at its northern part, something that had already been noted during the previous campaign period.

The significant decrease of the ground deformation observed at our GPS stations during the last two campaigns (June to December 2012) is more clearly depicted by the raw time series of the CGPS stations (Fig. 16). It is obvious that a substantial change in the amplitudes and directions of the velocity vectors is detected after February 2012, when also the abrupt micro-seismicity decrease took place in the caldera (Fig. 2). It therefore appears that the dynamic forces of the system have been calmed, but the attained uplift (>60 mm) remains without showing any signs of recovery (subsidence). Nevertheless, after early November 2012, a small amplitude change (uplift) in the vertical component at the stations SANT, MOZI, and NOMI is detected (Fig. 16), also observed at our campaign stations at the NE part of the caldera across the Columbo Line (Fig. 15b).

4.3. The Mogi modeling

The radial type of deformation observed particularly at the northern part of the caldera deduced by both the SqueeSAR analysis and the DGPS results (period 2011 to June 2012) constitutes a typical case of a magma influx at a certain depth producing this deformation

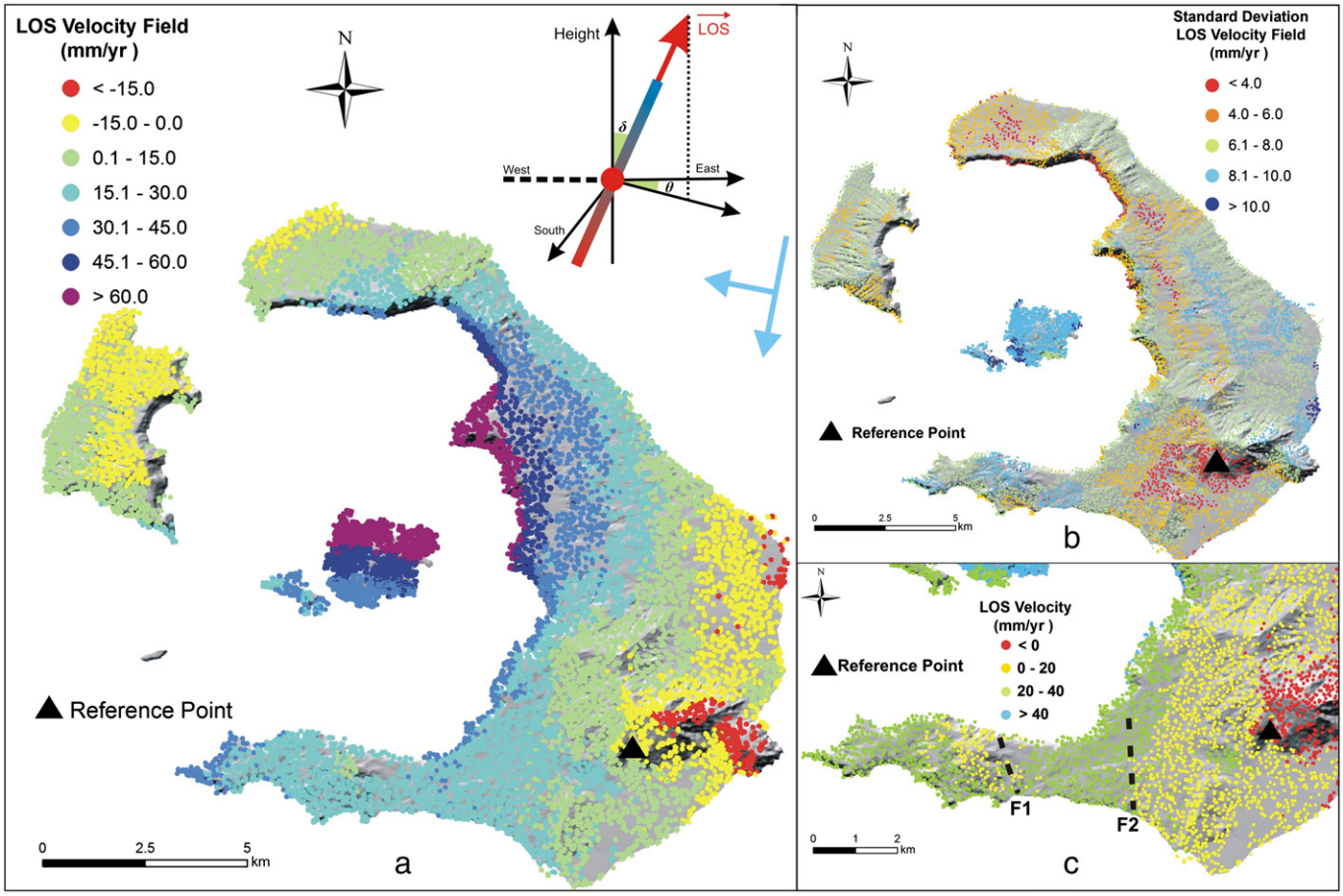

Fig. 11. (a) Ground LOS velocity (mm/yr) map for the *unrest* period April 2011 to March 2012 ($\delta \approx 39^{o}, \theta \approx 11^{o}$); (b) Standard deviation of the LOS velocity field; (c) LOS velocity field focusing at the southern part of Thera (different colored scale).

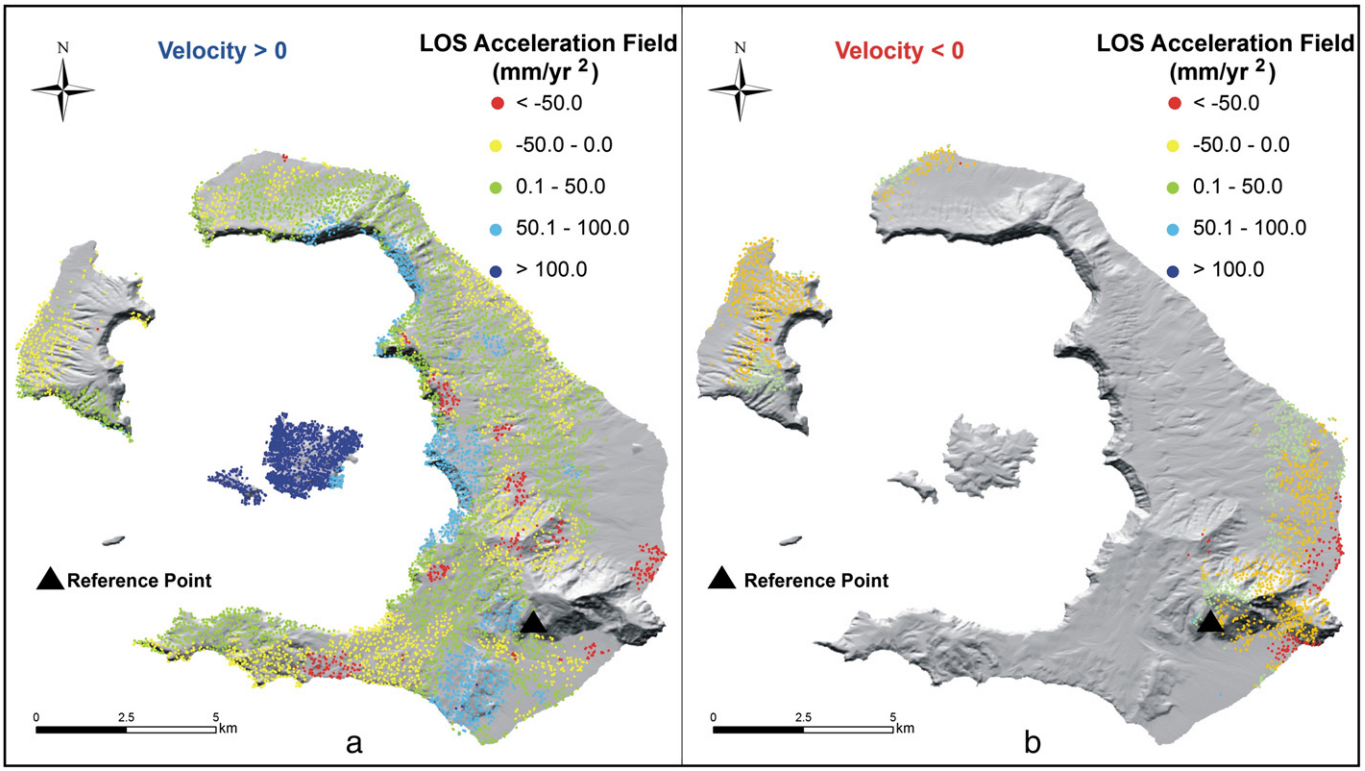

Fig. 12. Acceleration field for the *unrest* period April 2011 to March 2012 for (a) positive, and (b) negative LOS velocity values.

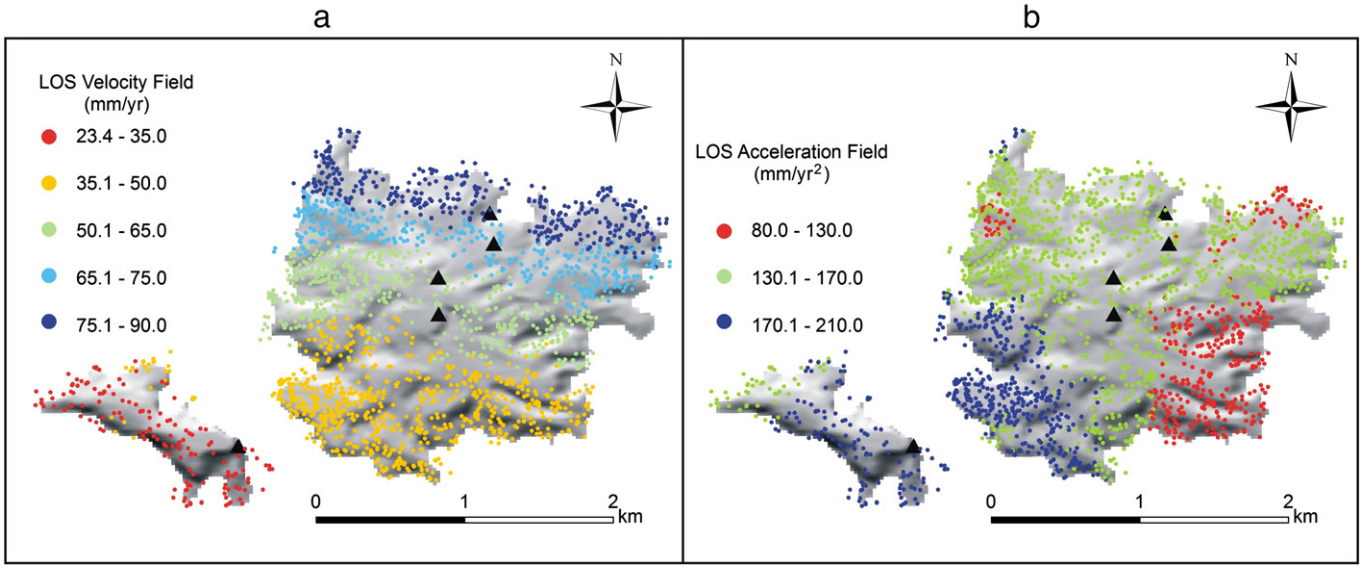

Fig. 13. (a) LOS velocity field (mm/yr), and (b) Acceleration field (mm/yr^2) focusing in the Kammenis for the *unrest* period. Triangles indicate GPS stations.

represented by an expanding Mogi point source (Mogi, 1958). Modeling attempts were performed to determine if pressure changes in the high-level magma chamber could account for the observed deformation. The "Mogi model" (Mogi, 1958) was adopted which assumes a small volume sphere of varying pressure, considered as a point source within an elastic half-space (where Poisson's ratio = 0.25), such that the elastic Lame coefficients λ and μ are equal. The resultant deformation on the ground surface is radially symmetric and the horizontal radial displacement, r, and the vertical displacement, z, are respectively given by (cylindrical polar coordinates):

$$r = C \cdot r / \left(d^2 + r^2\right)^{3/2} \quad (1)$$

$$z = C \cdot d / \left(d^2 + r^2\right)^{3/2} \quad (2)$$

where d is the source depth, r the horizontal distance from the source, and C is the so called *source strength parameter* (Sigmundsson, 1995) given by:

$$C = 3R^3P/4\mu \quad (3)$$

where P is the pressure change within the sphere, R is the radius of the sphere, and μ is the rigidity of the crust surrounding the sphere. Eq. (3) may also be presented as a function of volume change (V) at depth (McTigue, 1987):

$$V/\pi = R^3P/\mu. \quad (4)$$

The Mogi model was applied to calculate the displacements in GPS stations and PS/DS points deduced from the interferometric analysis at varying depths and locations at the northern inter-caldera part. The potential location of the source in between Thera, Therassia and Nea Kammeni was primarily determined by the observed pattern of deformation in both interferometric and GPS techniques.

The GPS remeasurement period Sept. 2011 to June 2012 was chosen for the modeling with respect to no. 07 station (Fig. 17). The Mogi model was applied to calculate the *absolute* displacements of our control (GPS) points for the hypothetical point source at varying depths and locations in the northern inter-caldera part. Applying the same methodology as Sigmundsson (1995), the residuals of the observed and predicted *absolute* displacements (vertical and horizontal) were determined by least-squares minimization at varying values of depth and radius of the sphere associated with the source strength parameter. An area of 4 km × 4 km just north of Nea Kammeni was divided in cells, sized 200 m × 200 m, and a grid search method was applied to define the best location for the Mogi source. For each grid location the residuals of the observed and calculated displacements were determined on the basis of minimum misfits between observed and predicted (theoretical) displacements. The best fit depth and radius values were then used to repeat the grid search on a denser grid of 100 m × 100 m to better improve the horizontal location of the best fit source, and for this improved location a new set of depth and radius values was finally determined. It was found that the best fit of the offshore source is located at coordinates [25° 23′ 19.774″ E, 36° 25′ 33.352″ N] in WGS'84 datum, at a depth of 4900^{+500}_{-500} m, and $V = 8.2^{+2.9}_{-1.0} \times 10^6$ m^3 shown in Fig. 17 and with respect to ITRF2008. Generally, a fairly good match was achieved for most of the stations, particularly for the horizontal component, even though the calculated vertical components seem to be higher than the observed ones.

The algorithm of Feigl and Dupre (1999) based on the formulation of dislocation along a fault (Okada, 1985) was used for the interferometric modeling taking into consideration the LOS direction and determining its unit vector (normalized to unit length) $\hat{s}$ (N: −0.12249, E: 0.61775, H: 0.77677). In our case, only the tensile component U_3 (>0) of the slip vector $\mathbf{U} = [U_1, U_2, U_3]$ was considered, representing an extension of a dyke that has equal dimensions in both directions (length along strike taken clock-wise from north, that is 0°; and width along dip from horizontal that is also 0°), acting thus as a homogenous expanding point source producing a radial type of deformation similar to a Mogi source.

The LOS deformation (Fig. 18a) for the period of the interferometric processing (April 2011–March 2012) was used for the modeling. The same procedure as in the GPS data previously described was applied to define the best fit parameters for the deformation source. It was found that the offshore magma source was located at coordinates [25° 23′ 43.1″ E, 36° 25′ 34.4″ N] in WGS'84 datum, at a depth of 4500^{+1700}_{-500} m and a volume $V = 9.2^{+3.2}_{-1.0} \times 10^6$ m^3 (Fig. 18b). The residuals between the observed and calculated values, as well as the histogram showing their distribution is also shown (Fig. 18c). Fig. 18d shows the variation between the effective magma volume and depth for the best-fit location. A fairly good fit was observed at only the northern part of the caldera. The largest residual values were met at the southeastern and southern part of Thera associated with the areal extent of the Alpine basement, and the depression

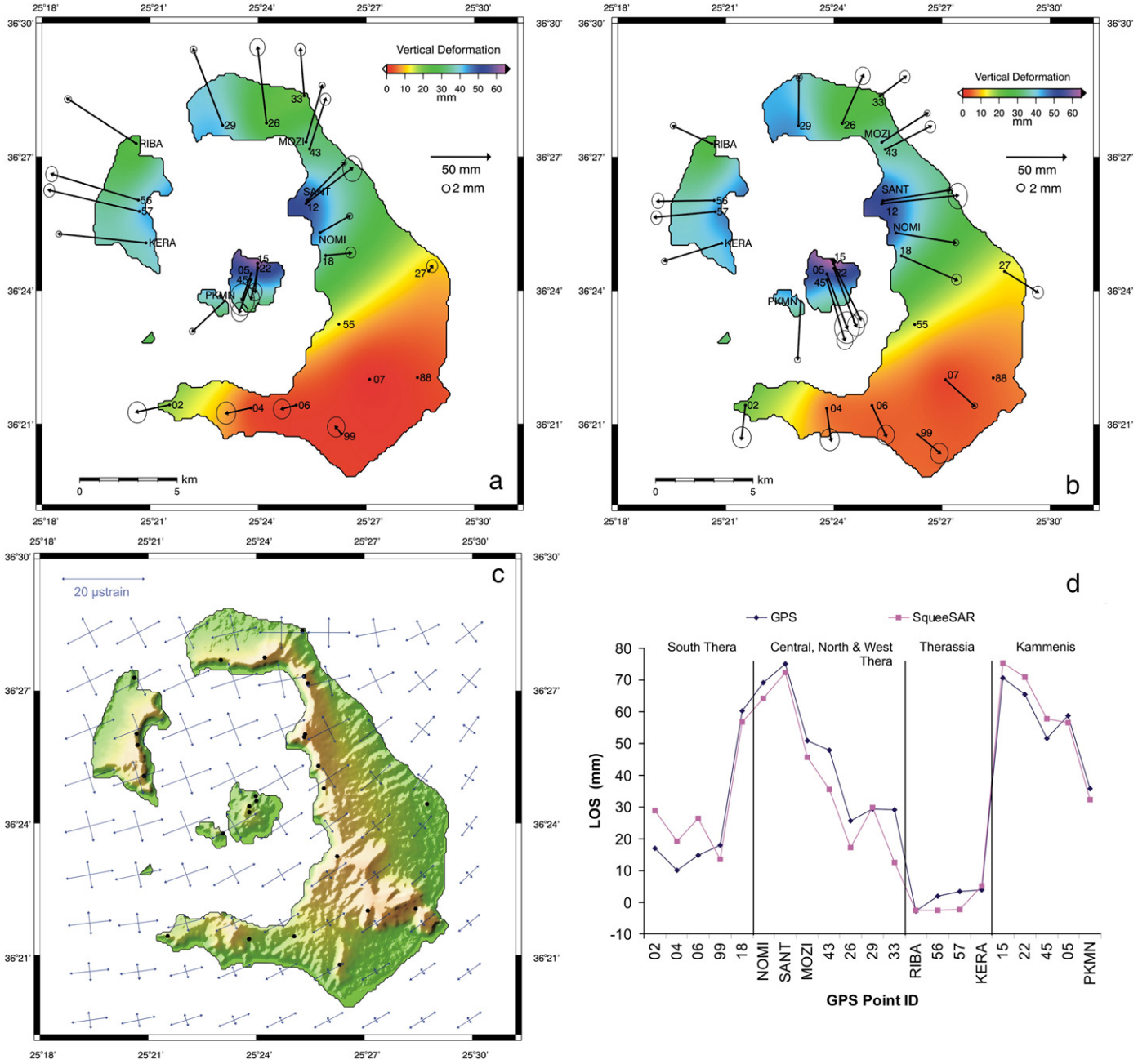

Fig. 14. GPS ground displacement maps (mm) for the period Sept. 2011 to June 2012, referred to (a) no. 07 local reference station; (b) ITRF2008; (c) Strain field (μstrain) deduced from the DGPS measurements; (d) Diagram showing comparison between GPS vectors projected on the LOS direction and the corresponding PS/DS vectors (rms = 7.3 mm).

zone in Akrotiri area. The latter possibly indicates that these parts of Thera might have not been largely affected by the exerting pressure of the magma chamber (as happens on the northern part of the caldera), and the observed deformation deduced by the InSAR analysis (Fig. 18a) should rather be attributed to the local tectonic characteristics.

It was found that the location of the InSAR modeled source is about 600 m east of the one determined by the DGPS modeling, but within the error area defined by the normalized χ^2 contour (at a 90% confidence level; Fig. 17a, red contour line). The former could mostly be attributed to the SAR satellite acquisition geometry, resulting in the loss of a realistic estimation of the N–S deformation component and the resultant elongation of the estimated error area along the E–W axis (Fig. 18b). A small discrepancy was also found in the values of depth (400 m) and volume (1×10^6 m^3) of the two modeled sources; these should be attributed to different time periods that the DGPS (Sept. 2011 to June 2012) and interferometric (April 2011 to March 2012) data-sets cover.

The above modeling results are consistent with previously published models by Newman et al. (2012) based on GPS results, and Parks et al. (2012) using interferometric data. All these models (including ours) fall within an area of less than 1 km diameter just north of Nea Kammeni. Discrepancies in depth and volume calculations between these models should be attributed to different type of data (GPS/InSAR), and different spanning periods of the used data-sets. However, comparing our interferometric modeling with a similar one by Papoutsis et al. (2012), larger discrepancies in the Mogi source parameters are noted, especially in their volume (24.2×10^6 m^3) determination. The latter may be explained as due to the different implemented approach on the interferometric analysis relating to the choice of the reference point located at the

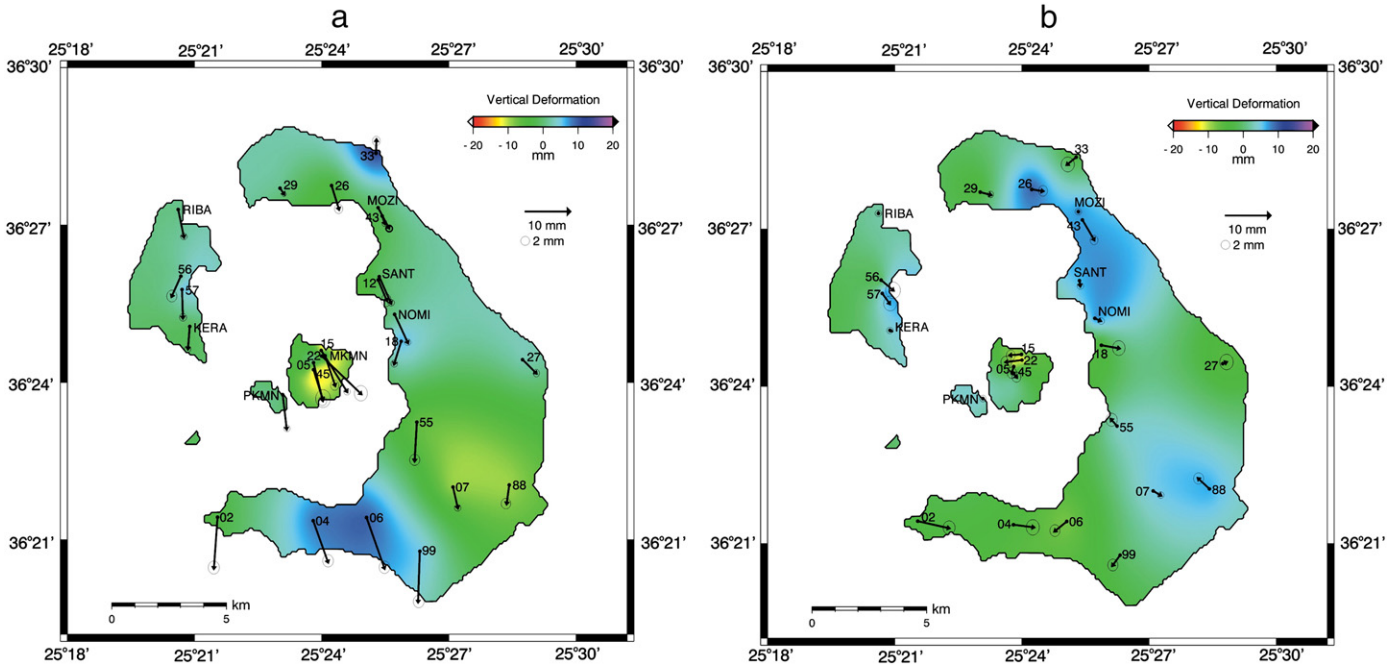

Fig. 15. (a) GPS ground deformation map for the period June to Sept. 2012 (ITRF2008); (b) GPS ground deformation map for the period Sept. to Dec. 2012 (ITRF2008).

northern part of the caldera (Mozi, Fig. 14), an area exhibiting strong *non-linear* deformation (84.1 mm/yr LOS after Papoutsis et al., 2012), and thus causing an overestimation of the observed LOS velocity values. Our reference point is located in the most stable area of the SVC, showing a *linear* motion even throughout the *unrest* period (10.5 mm/yr projected in LOS direction, Fig. 9), and leading to a more realistic LOS velocity field. Finally, Papageorgiou et al. (2012), dealing with InSAR for the short period March to December 2011 without presenting any model, are mainly focusing on the deformation in Nea Kammeni. They also calculate a subsidence of 5 mm/yr in Nea Kammeni before the unrest period, 1992–2010.

5. Discussion–Conclusions

The present study tries to present an integrated ground deformation picture applying state-of-the-art methodologies for the past twenty years. One of the main tasks of this effort is to demonstrate and comprehend the particular ways that SVC is deforming during a long observational period of quiescence from which important tectonic implications may be derived associated with its main characteristic features (e.g. Kammenis, Columbo and Kammenis zones). Therefore, the detailed ground deformation study on a millimeter-accuracy level may be proved very useful in identifying patterns of consistent behavior that may be correlated and/or explained by known or unknown tectonic features (e.g. faults, Alpine basement extent) determined also by geophysical studies.

It was possible to determine the deformation amplitude along the caldera rims of Thera and Therassia (Fig. 4) with a millimeter-accuracy. Some of these areas have decreasing or increasing rates of deformation (Figs. 6 and 7). These deformation parameters are of particular importance in the study of the long-term stability of the cliffs along the Santorini Caldera. They may be probably related to landslides and rock falls in these areas, and may contribute to the understanding in associated geotechnical hazard assessment.

5.1. The period 1992–2010

During the dormant period up to January 2011, *small* deformation velocity values deduced by GPS and interferometric analysis were observed, which are of a *linear* character, as determined by the very low values of SqueeSAR standard deviation and acceleration fields. However, several important tectonic issues should be pointed out relating to this period 1992–2010.

Palaea and Nea Kammeni show a clear differentiation in the vertical pattern: Palaea Kammeni presents a continuous uplift (2 mm/yr) of increasing rate (Figs. 6b and 8a); the adjacent Nea Kammeni to its great extent basically subsides (up to −6 mm/yr) with its center subsiding slower than its margins (Figs. 4, 8a and 10). The subsidence taking place in Nea Kammeni (Fig. 8a) has a strong E–W kinematic influence observed in the islet (Fig. 8b), as has been described analytically and also shown by the DGPS results (Table 3; Fig. 10).

The opposite vertical motion between the Palaea and Nea Kammeni (Figs. 4 and 8a) may indicate a possible surface kinematic boundary/fault (?) in between these islets (see broken line in Fig. 1), constituting possible extension of the NW–SE trending fault east of Therassia. This boundary may extend further to the SE, crossing the Akrotiri area, marking thus the western part of the SVC. The latter may also be supported on the basis of:

(i) the direction of our GPS velocity vectors in Therassia and Akrotiri area (Table 3; Fig. 10) uniformly pointing to NW,
(ii) the deeper Audio-Magnetotelluric (AMT) induction vectors (0.1–0.5 Hz) resulted from an older geothermal study in the broader area of Akrotiri (Papageorgiou et al., 2010; Sotiropoulos et al., 1996), where a fault is inferred, and
(iii) the eastern limit of the gravity low (110 mGal), shown on the Santorini gravity anomaly map (Fig. 3), associated with a possible location of a faulting feature in the underlying basement (F1; Fig. 1), verifying the above AMT interpretation.

The above invoked kinematic boundary may be resolved by a more accurate gravity anomaly map of the area with denser offshore/inter-caldera spatial gravity station coverage.

Another significant outcome of the east–west component of the SqueeSAR image (Fig. 8b) is the profound kinematics resulted across the Columbo fracture zone, where its western part encompassing all the northern part of Thera shows a clear westward motion resulted also by the DGPS (Fig. 10). Assuming that the Columbo Zone is part of the major regional NE–SW trending Anhydros Basin Fault System

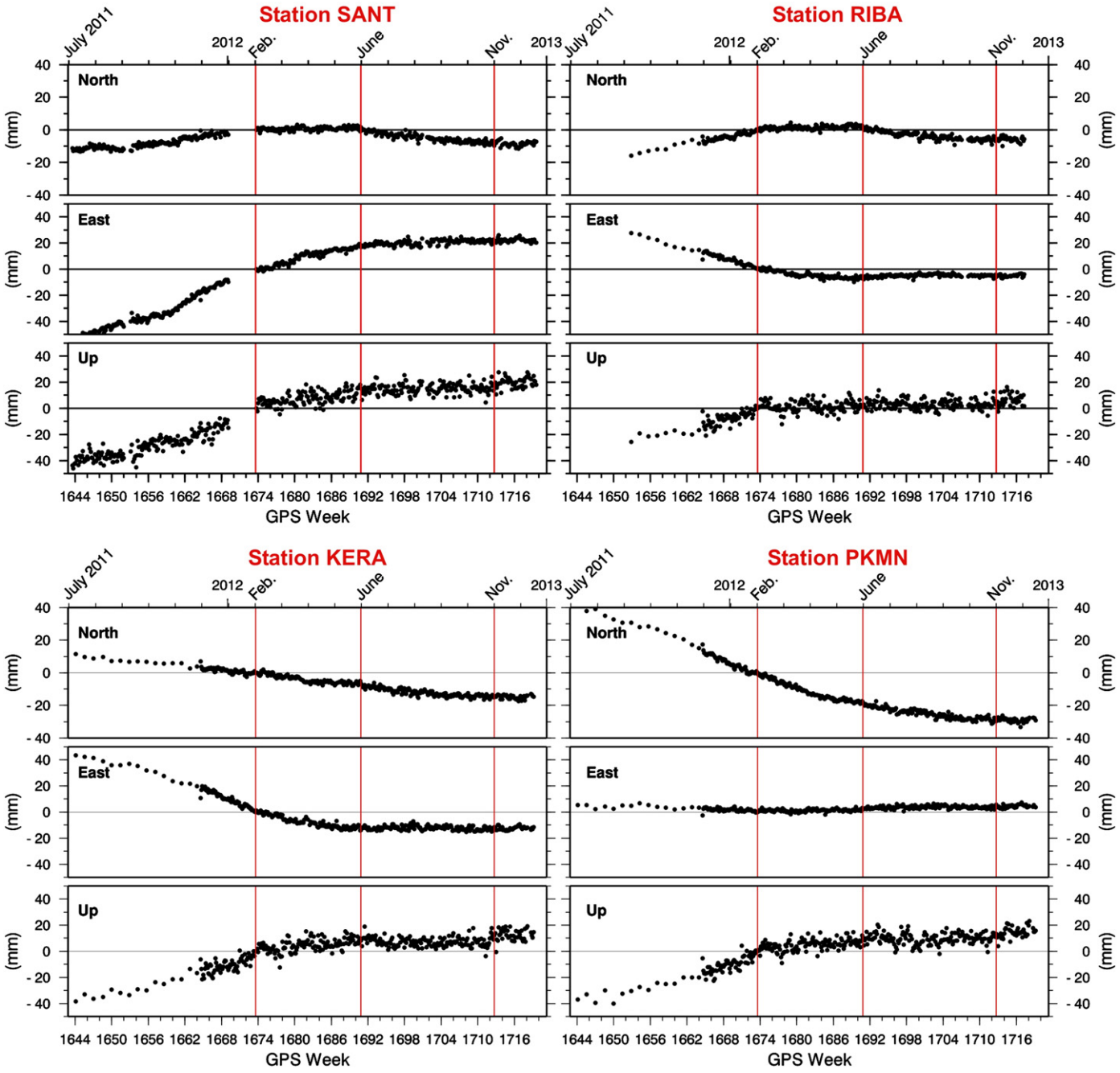

Fig. 16. Raw Time Series of the three components for four selected CGPS stations for the period July 2011 to end December 2012.

(i.e. Dimitriadis et al., 2009; Nomikou et al., 2012b; Sakellariou et al., 2010) NE of Thera, it therefore constitutes not only a weak zone that most probably extends in the caldera, but also a significant faulting feature at the northern part of Thera that seems to control the deformation across its sides.

Another issue relating to the tectonics of the SVC is the outcropping Alpine basement at Monolithos (Fig. 1) which is not an isolated limestone block, but it seems to constitute a continuous part of the Thera basement, as it is indicated by the gravity anomaly map (Fig. 3), and also supported by the GPS and interferometric results showing similar kinematic characteristics as the southerly main outcrop basement unit.

Generally, the ground deformation during the period 1992 to 2010 was of linear character associated with small velocity and acceleration values without any indication of a magmatic activity. Previous work though by Stiros et al. (2010) and Saltogianni and Stiros (2012) has invoked a "partial caldera inflation that was assigned to a slow magma intrusion" based on the increased length ($\approx$100 mm) of the EDM base-lines in the northern part of the caldera, for the period 1994–2000. However, the latter is not fully supported from our data (Figs. 8 and 10): It is observed that Nea Kammeni (where the EDM reference station was located) was continuously subsiding by about 6 mm/yr (moving to SW) with respect to station no. 07, and about 8 mm/yr with respect to ITRF. Therassia was moving (away from the Kammenis) to NW by about 2 mm/yr and about 1 mm/yr of vertical velocity (Figs. 8 and 10), indicating thus a lengthening of the EDM base-lines and a clear extension of the region between these two islets by an estimated amplitude of about 43 mm for a six-year period. Therefore, it is not clear whether the extension between Nea Kammeni and Therassia disputes the interpretational approach of the invoked small-scale inflation event; nevertheless it certainly decreases its magnitude. Considering also our PS/DS time series in Therassia and Nea

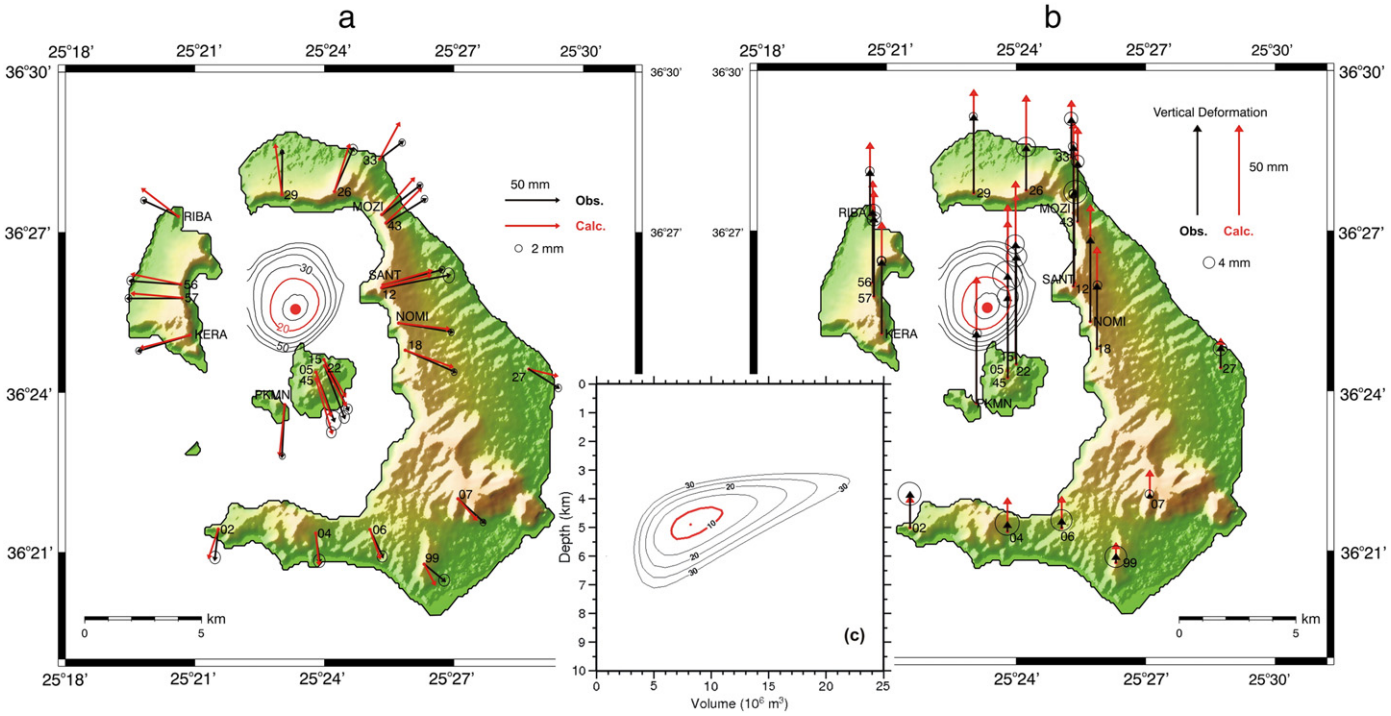

Fig. 17. Mogi modeling of the observed (*black arrows*) and calculated (*red arrows*) of the GPS displacements for the period Sept. 2011 to June 2012 for (a) Horizontal and (b) Vertical components. *Red dot* indicates the location of the best-fit Mogi source. (c) Diagram between depth and volume variation for the best fit location. Normalized χ^2 error contours are also shown; *red contour line* indicates the 90% confidence level for the location estimate, and 95% confidence level for the Volume vs Depth estimates.

Kammeni for the period 1994–2000, there is not any certain indication or evidence of an irregular deformation.

It is evident that during the *quiet* period (1992–2010), all seismic energy release was taking place around the Columbo area with negligible inter-caldera activity (Fig. 2a), while the *unrest* period initiated with the occurrence of small magnitude earthquakes inside the caldera and increasing number of events (Fig. 2b).

5.2. The period 2011–June 2012

During the *unrest* period between January 2011 and January 2012, the strong ground deformation was mainly of high amplitude at the northern part of the caldera. The gradual deformation with increasing rate in Nea Kammeni (Fig. 13) as determined by the SqueeSAR analysis is clearly verified here considering our four GPS stations in the islet, where the Up component gradually decreases from north to south; that is from ≈65 mm (no. 15) to ≈46 mm (no. 45) — (Table 3; Fig. 14). The horizontal vectors are of almost N–S direction. This type of motion can hardly be detected by the interferometric technique (due to satellite trajectory), the deformation therefore depicted in Nea Kammeni by SqueeSAR (Fig. 13) should mostly be attributed to the vertical component. Palaea Kammeni shows a south-westward motion (≈50 mm) having thus a significant west component (Fig. 14). The latter may explain the reduced LOS velocity values observed in Palaea Kammeni when compared to Nea Kammeni (Fig. 13a), since a westward-negative component (motion away from satellite) is now added to the prevailing strong upward-positive component (motion towards the satellite).

A strong northward motion based on GPS is observed in the northern part of Thera and to the west of the Columbo Zone, ranging from 28 mm (no. 33) to 42 mm (no. 29), while north-eastward to eastward motions prevail east of that zone (43–57 mm) — Fig. 14. Because of the orientation of these vectors, lower LOS velocity values are observed in the SqueeSAR image (Fig. 11) in the northern part of Thera, while higher LOS velocity values are observed east of the Columbo zone, where the motion is toward the satellite (positive values).

W-NW ground displacements are observed in Therassia with amplitudes up to 60 mm (Fig. 14; Table 3). Therefore, because of that westward ground motion shown on the GPS displacement map, the negative LOS velocity values (motion away from satellite) in the SqueeSAR image can easily be explained.

A belt area encompassing Monolithos and the main basement outcrop to the south is described by negative LOS velocity values (Fig. 11). A similar pattern is also observed from the GPS results (Fig. 14a) for the same area. However, the increased negative LOS velocity values (red circles in Fig. 11) associated mainly with the cliffs of the outcrops is difficult to be interpreted taking into consideration that small LOS velocity values (−1 to +1 mm/yr) were measured for the previous *quiet* period (Fig. 4a).

The results of the source modeling parameters deduced independently by GPS and interferometric data are within the error limits of both modeling procedures. Their joint interpretation defines an area, depth and volume of a magma source which is consistent with previous works, as analytically has been described above. The deviations between observed and calculated deformation values noticed mainly at the southern part of Thera (Figs. 17 and 18) should rather be attributed to the local geological/tectonic characteristics of this area. It appears that the deformation taking place at the northern inter-caldera area due to the magma influx at depth does not equally affect the SE part of Thera, where the Alpine basement may be acting as an effective resistive boundary to the exerting radial source strength field. The latter may be recognized at Fig. 14c, where the NW–SE trending axis (coinciding with the radial type of deformation due to Mogi source) is becoming significantly smaller toward the south.

5.3. The period June–December 2012

Regarding the latest state of the SVC, it is evident that the bulging associated with an intense radial deformation that started at the

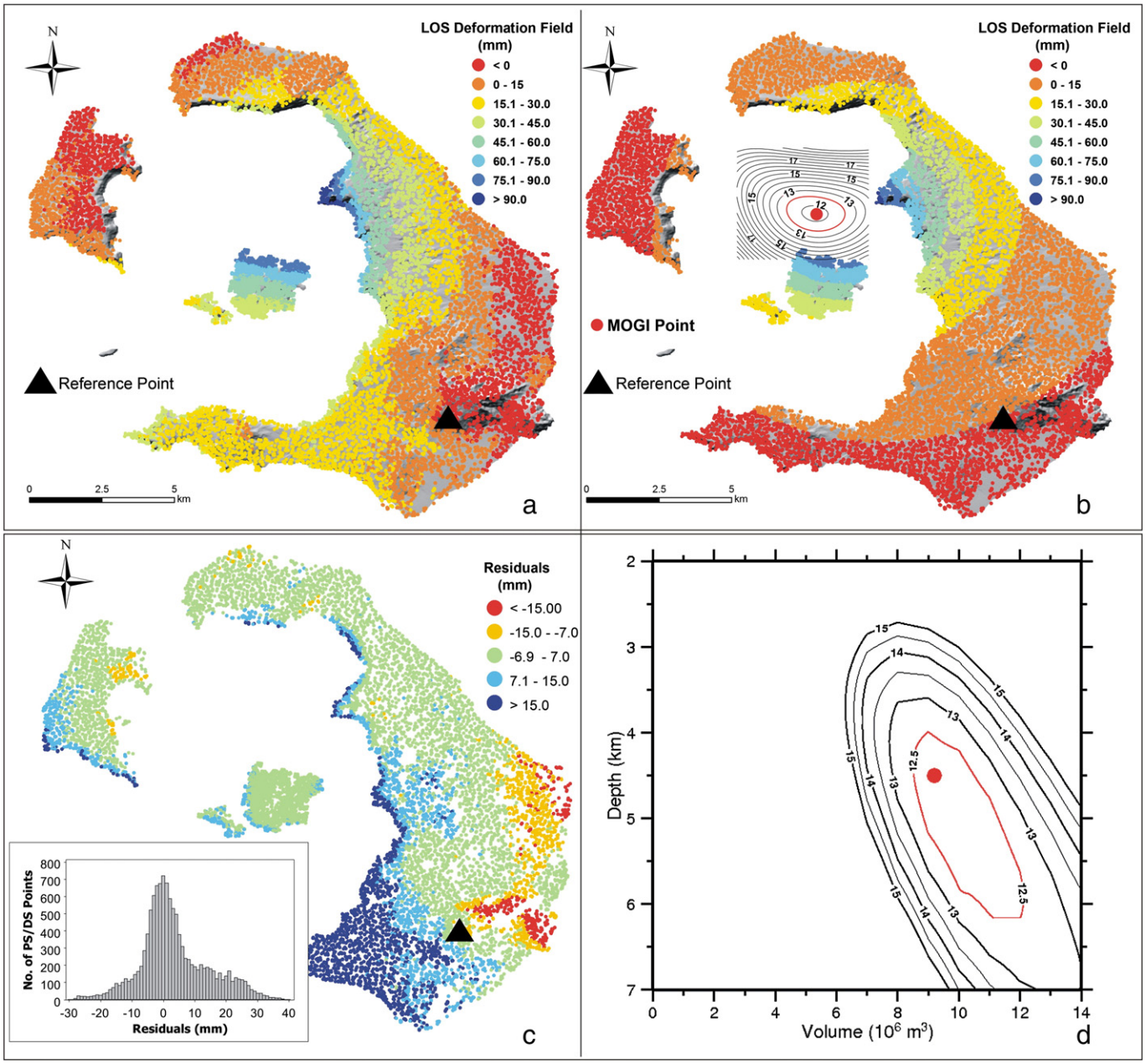

Fig. 18. SqueeSAR Mogi modeling for the period April 2011 to March 2012. (a) Observed LOS deformation field (mm); (b) Calculated LOS deformation field showing also the location (*red dot*) of the best-fit source, together with the normalized χ^2 error contour lines; (c) Map of residuals (in mm) between observed and calculated values, together with their histogram distribution; (d) Diagram between depth and volume variation for the best fit location. *Red contour lines* indicate the 90% confidence level.

northern part of the caldera in early 2011 continued up to February 2012; afterwards its rate declined, and after late May to end 2012 it seemed to have stopped (Fig. 16). At the same period, the inter-caldera seismicity had dramatically increased, dying out after February 2012 (Fig. 2b). A drastic change was also observed on the horizontal deformation vectors after February 2012, as deduced by CGPS data (Fig. 16) and campaign data (Fig. 15) with a major alteration in both amplitude and direction, not presenting a radial deformation pattern any longer. The latter therefore is suggesting that the upward intruded magma from a deeper reservoir (Hooper, 2012; Parks et al., 2012) that took place mainly in 2011 has rather settled in some ways; the exerted pressure has declined, reducing thus the deformation vectors observed at DGPS/CGPS stations. The identified faults (Fig. 1), as constituting weak zones in the upper crust, may play an important role in the horizontally magma settlement (in the form of dykes/sills) that could reduce the pressure in the shallower magma chamber. The slight change with a tendency to uplift observed in the northern part of the caldera during the most recent GPS remeasurement period (Sept. to Dec. 2012) needs more time and attention to see how it evolves in the future. This was also recorded at CGPS stations since early November 2012 (Figs. 15b and 16), without any noticeable change in the seismic activity (Fig. 2b). The correlation between the recorded micro-seismicity and observed deformation, as well as the role of the major and minor tectonic features requires precise investigation for the better understanding of the behavior of the SVC during unrest periods.

If an eruption might take place during the next few years, it is estimated that it should be rather a similar one as the 1925–1928 or 1953 eruption (Georgalas, 1953; Ktenas, 1927; Pyle and Elliott, 2006; Reck, 1936) with emissions of ash and gas plumes, including

the ejections of ballistics. However, any upward influx of magma into a shallow magma chamber, which depends on unforeseen dynamics at the deeper crustal magma reservoir and the tectonic environment (e.g. stress field at time), will occur sporadically and uncontrolled (Hooper, 2012). Therefore, the continuation of the multi-disciplinary surveillance of the Santorini Volcano is imperative with concentrated application of all state-of-the-art geological and geophysical methodologies.

Acknowledgments

We thank the European Space Agency (ESA) for providing radar data (C1P 9499), the Hellenic Forestry Commission for providing GPS receivers, and Mr. S. Chailas for his contribution in the gravity data analysis. CGPS data of NOMI, MOZI, KERA, RIBA, MKNM and PKMN stations were provided by the *UNAVCO* Organization (www.unavco.org) with the support of the Georgia Institute of Technology (Prof. A. Newman) and University of Patras (Prof. S. Stiros). Generic mapping tool (GMT) used to generate some of the figures. The Earthquake Planning and Protection Organization of Greece financed the last GPS survey.

Appendix A. Supplementary data

Supplementary data associated with this article can be found in the online version, at http://dx.doi.org/10.1016/j.tecto.2013.03.012. These data include Google maps of the most important areas described in this article.

References

Amelung, F.S., Jonsson, S., Zebker, H., Segall, P., 2000. Widespread uplift and 'trapdoor' faulting in Galapagos volcanoes observed with radar interferometry. Nature 407, 993–996. http://dx.doi.org/10.1038/35039604.

Astronomical Institute, University of Berne, 2001. Bernese GPS Software Version 4.2. In: Hugentobler, U., Schaer, S., Fridez, P. (Eds.), (515 pp.).

Bohnhoff, M., Rische, M., Meier, T., Endrun, B., Harjes, H.-P., Stavrakakis, G., 2004. A temporary seismic network on the Cyclades (Aegean Sea, Greece). Seismological Research Letters 75/3, 352–357.

Bohnhoff, M., Rische, M., Meier, T., Becker, D., Stavrakakis, G., Harjes, H.P., 2006. Microseismic activity in the Hellenic Volcanic Arc, Greece, with emphasis on the seismotectonic setting of the Santorini–Amorgos zone. Tectonophysics 423 (1–4), 17–33.

Bond, A., Sparks, R.S.J., 1976. The Minoan eruption of Santorini, Greece. Journal of the Geological Society of London 132, 1–16.

Bonforte, A., Guglielmino, F., Cortelli, M., Ferretti, A., Puglisi, G., 2011. Structural assessment of Mount Etna from permanent scatterers analysis. Geochemistry, Geophysics, Geosystems 12, Q02002. http://dx.doi.org/10.1029/2010GC003213.

Briole, P., Massonnet, D., Delacourt, C., 1997. Post-eruptive deformation associated with 1986–87 and 1989 lava flows of Etna detected by radar interferometry. Geophysical Research Letters 24, 37–40. http://dx.doi.org/10.1029/96GL03705.

Burgmann, R.G., Hilley, A., Ferretti, A., Novali, F., 2006. Resolving vertical tectonics in the San Francisco Bay area from GPS and Permanent Scatterer InSAR analysis. Geology 34, 221–224.

Cascini, L., Fornaro, G., Peduto, D., 2010. Advanced low- and full-resolution DInSAR map generation for slow-moving landslide analysis at different scales. Engineering Geology 112 (1–4), 29–42.

Chailas, S., Tzanis, A., Lagios, E., 2012. Santorini Volcanic Complex internal structure detected by gravity and magnetotelluric data interpretation. Volcanism of the Southern Aegean in the Frame of the Broader Mediterranean Area (VOLSAM 2012), 10–12 October 2012, Santorini Island, Greece.

Chouliaras, G., Drakatos, G., Makropoulos, K., Melis, S., 2012. Recent seismicity detection increase in the Santorini Volcanic Island Complex. Natural Hazards and Earth System Sciences 12, 859–866.

Dach, R., Hugentobler, U., Fridez, P., Meindl, M., 2007. Bernese GPS Software Version 5.0. Astronomical Institute, University of Bern, Bern.

Delibasis, N., Sahpazi, M., Chailas, S., Karantonis, G., 1995. Micro-earthquake activity of the Santorini Volcanic Islands during period 1985–1989. Annales Geologiques de Pays Helleniques 36, 181–207.

Dietrich, V.J., 2004. Die Wiege der abendländischen Kultur und die minoische Katastrophe – eine Vulkan verändert die Welt. Neujahrsblatt (Naturforschende Gesellschaft in Zürich) 207, 93 S (Stück).

Dimitriadis, I., Karagianni, E., Panagiotopoulos, D., Papazachos, C., Hatzidimitriou, P., Bohnhoff, M., Rische, M., Meier, T., 2009. Seismicity and active tectonics at Columbo Reef (Aegean Sea, Greece): monitoring an active volcano at Santorini Volcanic Center using a temporary seismic network. Tectonophysics 465, 136–149.

Druitt, T.H., Francaviglia, V., 1992. Caldera formation on Santorini and the physiography of the islands in the late Bronze Age. Bulletin of Volcanology 54, 484–493.

Druitt, T.H., Mellors, R., Pyle, D., Sparks, R., 1989. Explosive volcanism on Santorini, Greece. Geological Magazine 126, 95–213.

Druitt, T.H., Edwards, L., Mellors, R.A., Pyle, D.M., Sparks, R.S.J., Lanphere, M., Davies, M., Barriero, B., 1999. Santorini Volcano. Geological Society Memoir 19, 165.

Druitt, T.H., Costa, F., Deloule, E., Dungan, M., Scaille, B., 2012. Decadal to monthly timescales of magma transfer and reservoir growth at a caldera volcano. Nature 482, 77–80.

Farmer, G., Newman, A., Psimoulis, P., Stiros, S., 2007. Geodetic characterization of Santorini Caldera from continuous GPS measurements. Abstract G43B-1195, AGU-2007 Fall Meeting.

Feigl, K., Dupre, E., 1999. RNGCHN: a program to calculate displacement components from dislocations in elastic half-space with applications for modelling geodetic measurements of crustal deformation. Computers & Geosciences 25 (6), 695–704.

Feng, G., Jónsson, S., 2012. Shortcomings of InSAR for studying megathrust earthquakes: the case of the Mw9.0 Tohoku-Oki earthquake. Geophysical Research Letters 39 (10) art. no. L10305.

Ferretti, A., Prati, C., Rocca, F., 1999. Non-uniform motion monitoring using the permanent scatterers technique. Proc. 2nd Int. Workshop ERS SAR Interferometry, FRINGE, Liège, Belgium, Nov. 10–12, pp. 1–6.

Ferretti, Prati, C., Rocca, F., 2000. Non-linear subsidence rate estimation using permanent scatterers in differential SAR interferometry. IEEE Transactions on Geoscience and Remote Sensing 38 (5), 2202–2212.

Ferretti, A., Prati, C., Rocca, F., 2001. Permanent scatterers in SAR interferometry. IEEE Transactions on Geoscience and Remote Sensing 39 (1), 8–20.

Ferretti, A., Fumagalli, A., Novali, F., Prati, C., Rocca, F., Rucci, A., 2011. A new algorithm for processing interferometric data-stacks: SqueeSAR. IEEE Transactions on Geoscience and Remote Sensing. http://dx.doi.org/10.1109/TGRS.2011.2124465.

Floyd, M.A., Billiris, H.D., Paradissis, D., Veis, G., Avallone, A., Briole, P., McClusky, S., Nocquet, J.M., Palamartchouk, K., Parsons, B., England, P.C., 2010. A new velocity field for Greece: implications for the kinematics and dynamics of the Aegean. Journal of Geophysical Research 115, B10403. http://dx.doi.org/10.1029/2009JB007040.

Francalanci, L., Vougioukalakis, G., Perini, G., Manetti, P., 2005. A west–east traverse along the magmatism of the south Aegean volcanic arc in the light of volcanological, chemical and isotope data. The South Aegean Active Volcanic Arc: present knowledge and future perspectives. Developments in Volcanology 7, 65–111.

Funning, G.J., Burgmann, R., Ferretti, A., Novali, F., 2007. Creep on the Rodgers Creek Fault, northern San Francisco Bay area from a 10-year PSInSAR data set. Geophysical Research Letters 34, L19306. http://dx.doi.org/10.1029/2007GL030836.

Fytikas, M., Innocenti, F., Manetti, P., Mazuoli, R., Peccerilo, A., Villari, L., 1984. Tertiary to Quaternary evolution of the volcanism in the Aegean Region. In: Dixon, J.E., Robertson, A.H.F. (Eds.), The Geological Evolution of the Eastern Mediterranean: Geol. Soc. London, Spec. Pub., 17, pp. 687–699.

Ganas, A., Parsons, B., 2009. Three-dimensional model of Hellenic Arc deformation and origin of the Cretan uplift. Journal of Geophysical Research 114, B06404. http://dx.doi.org/10.1029/2008JB005599.

Georgalas, G., 1953. L' eruption du volcan de Santorini en 1950. Bulletin of Volcanology 13, 39–55.

Georgalas, G., Papastamatiou, J., 1953. L' eruption du volcan du Santorini en 1939–41. Eruption du dome Fouque. Bulletin of Volcanology 13, 3–18.

Hanssen, R.F., 2001. Radar Interferometry: Data Interpretation and Error Analysis. Kulver Academic Publisher (308 pp.).

Heiken, G., McCoy, F., 1984. Caldera development during the Minoan eruption, Thera, Cyclades, Greece. Journal of Geophysical Research 89, 8441–8462.

Heiken, G., McCoy, F., 1990. Precursory activity to the Minoan Eruption, Thera, Greece. In: Hardy, D., Keller, J., Galanopoulos, V., Fleming, N., Druitt, T. (Eds.), Thera and the Aegean World III: The Thera Foundation, London, 2, pp. 79–88.

Hollenstein, Ch., Müller, M.D., Geiger, A., Kahle, H.-G., 2008. Crustal motion and deformation in Greece from a decade of GPS measurements, 1993–2003. Tectonophysics 449, 17–40.

Hooper, A., 2012. A volcano's sharp intake of breath. Nature Geoscience. http://dx.doi.org/10.1038/ngeo1584.

Hooper, A., Segall, P., Zebker, P., 2007. Persistent scatterer interferometric synthetic aperture radar for crustal deformation analysis with application to Volcan Alcedo, Galapagos. Journal of Geophysical Research 112, B07407. http://dx.doi.org/10.1029/2006JB004763.

Jackson, J.A., 1994. Active tectonics of the Aegean region. Annual Review of Earth and Planetary Sciences 22, 239–271.

Kahle, H.-G., Straub, C., Reilinger, R., McClusky, S., King, R., Hurst, K., Veis, G., Kastens, K., Cross, P., 1998. The strain rate field in the Eastern Mediterranean region, estimated by repeated GPS measurements. Tectonophysics 294, 237–252.

Kampes, B., 2006. Radar Interferometry: Persistent Scatterer Technique. Dordrecht. The Netherlands, The Netherlands.

Kolaitis, A., 2011. Tectonic and Volcanological study relating to the seismicity of Santorini. Doctorate Thesis, Dept. Geophysics-Geothermics, University of Athens (GR), 299 p.

Ktenas, K., 1927. L' eruption du volcan des Kammenis (Santorini) en 1925, II. Bulletin of Volcanology 4, 7–46.

Lagios, E., 1995. Microgravimetric monitoring of the Santorini Volcano, Greece. Proc. Intern. Workshop "New Challenges for Geodesy in Volcanoes Monitoring", June 14–16, 1993, Walferdange, Luxenburg: Tire a part des Cahiers du Centre Europeen de Geodynamique et de Seismologie, 8, pp. 293–305.

Lagios, E., Drakopoulos, J., Hipkin, R.G., Gizeli, K., 1988. Microgravimetry in Greece: applications to earthquake and volcano-eruption prediction. Tectonophysics 152, 197–207.

Lagios, E., Tzanis, A., Hipkin, R.G., Delibasis, N., Drakopoulos, J., 1989. Surveillance of Thera Volcano — monitoring of the local gravity field. Proc. 3rd Inter. Congr. "Thera and the Aegean World", Sept. 3–9, Santorini, Greece, pp. 216–223.

Lagios, E., Parcharidis, I., Foumelis, M., Sakkas, V., 2005a. Ground deformation monitoring of the Santorini Volcano using Satellite Radar Interferometry. Proc. 2nd International Conference on Recent Advances in Space Technologies, pp. 667–672.
Lagios, E., Sakkas, V., Parcharidis, I., Dietrich, V., 2005b. Ground deformation of Nisyros Volcano (Greece) for the period 1995–2002: results from DInSAR and DGPS observations. Bulletin of Volcanology 68, 201–214.
Lagios, E., Sakkas, V., Novali, F., Fumagalli, A., Del Conte, S., 2011. Ground deformation studies in Cephallonia Island (Western Greece) based on DGPS & PS interferometry. Geosciences & Remote Sensing Symposium (IGARSS) — 2011 IEEE International, Vancouver Canada. http://dx.doi.org/10.1109/IGARSS.2011.605008.
Lagios, E., Papadimitriou, P., Novali, F., Sakkas, V., Fumagalli, A., Vlachou, K., Del Conte, S., 2012. Combined seismicity pattern analysis, DGPS and PSInSAR studies in the broader area of Cephalonia (Greece). Tectonophysics 524–525, 43–58.
Massironi, M., Zampieri, D., Bianchi, M., Schiavo, A., Frannceschini, A., 2009. Use of PSInSAR™ data to infer active tectonics: clues on the differential uplift across the Giudicarie belt (Central-Eastern Alps, Italy). Tectonophysics 476, 297–303.
Massonnet, D., Feigl, K.L., 1998. Radar interferometry and its application to changes in the Earth's surface. Reviews of Geophysics 36, 441–500.
McTigue, D.F., 1987. Elastic stress deformation near a finite spherical magma body: resolution of the point source paradox. Journal of Geophysical Research 92 (B12), 12,931–12,940.
Mercier, J.L., Sorel, D., Vergely, P., Simeakis, K., 1989. Extensional tectonic regimes in the Aegean basins during Cenozoic. Basin Research 2, 49–71.
Mogi, K., 1958. Relations between the eruptions of various volcanoes and the deformation of ground surfaces around them. Bulletin of the Earthquake Research Institute, University of Tokyo 36, 99–134.
Newman, A.V., Stiros, S., Feng, L., Psimoulis, P., Moschas, F., Saltogianni, V., Jiang, Y., Papazachos, K., Panagiotopoulos, D., Karagianni, E., Vamvakaris, D., 2012. Recent geodetic unrest at Santorini Caldera. Geophysical Research Letters. http://dx.doi.org/10.1029/2012GL051286.
Nomikou, P., Carey, S., Papanikolaou, D., Croff Bell, K., Sakellariou, D., Alexandri, M., Bejelou, K., 2012a. Submarine volcanoes of the Columbo Volcanic Zone NE of Santorini Caldera, Greece. Global and Planetary Change. http://dx.doi.org/10.1016/j.gloplacha.2012.01.001.
Nomikou, P., Papanikolaou, D., Alexandri, M., Sakellariou, D., Rousakis, G., 2012b. Submarine volcanoes along the Aegean Volcanic Arc. Sp. Issue Tectonophysics: "The Aegean: A Natural Laboratory for Tectonics". http://dx.doi.org/10.1016/j.tecto.2012.10.001.
Okada, Y., 1985. Surface deformation to shear and tensile faults in a half-space. Bulletin of The Seismological Society of America 75 (4), 1135–1154.
Papadimitriou, P., Kaviris, G., Voulgaris, N., Kolaitis, A., Karakonstantis, A., Kapetanidis, V., Makropoulos, K., 2012. Seismic monitoring of the Santorini Volcano. Abstracts Book, 33rd ESC General Assembly, Moscow, Russia, p. 132.
Papageorgiou, E., Tzanis, A., Sotiropoulos, P., Lagios, E., 2010. DGPS and magnetotelluric constraints on the contemporary tectonics of the Santorini Volcanic Complex. Bulletin of the Geological Society of Greece XLIII (1), 344–356.
Papageorgiou, E., Foumelis, M., Parcharidis, I., 2012. Long- and short-term deformation monitoring of Santorini Volcano: unrest evidence by DInSAR analysis. IEEE Journal of Selected Topics in Applied Earth Observations and Remote Sensing 5, 1531–1536.
Papazachos, K., Panagiotopoulos, D., Karagianni, E., Vamvakaris, D., Albanakis, K., Laopoulos, Th., Fytikas, M., 2012. The evolution of the 2011–2012 Santorini volcanic unrest as revealed by seismicity. Volcanism in the Southern Aegean in the Frame of the Broader Mediterranean Area (VOLSAM 2012). October 10–12, Santorini, Greece.
Papoutsis, I., Papanikolaou, X., Floyd, M., Ji, K.H., Kontoes, C., Paradissis, D., Zacharis, V., 2012. Mapping Inflation at Santorini Volcano, Greece, Using GPS and InSAR. http://dx.doi.org/10.1029/2012GL054137.
Parks, M., Biggs, J., England, P., Mather, T.A., Nomikou, P., Palamartchouk, K., Papanikolaou, X., Paradissis, D., Parson, B., Pyle, D.M., Raptakis, C., Zacharis, V., 2012. Evolution of Santorini Volcano dominated by episodic and rapid fluxes of melt from depth. Nature. http://dx.doi.org/10.1038/NGEO1562.
Peltier, A., Bianchi, M., Kaminski, E., Komorowski, J.C., Rucci, A., Staudacher, T., 2010. PSInSAR as a new tool to monitor pre-eruptive volcano deformation: validation using GPS measurements on Piton de la Fournaise. Geophysical Research Letters 37, L12301. http://dx.doi.org/10.1029/2010GL043846.
Perissoratis, C., 1995. The Santorini Volcanic Complex and its relation to the stratigraphy and structure of the Aegean Arc, Greece. Marine Geology 167 (3–4), 391–411.
Pesci, A., Teza, G., 2007. Strain rate analysis over the central Apennines from GPS velocities: the development of a new free software. Bollettino di Geodesia e Scienze Affini 56, 69–88.
Pyle, D., Elliott, J., 2006. Quantitative morphology, recent evolution, and future activity of the Kameni Islands Volcano, Santorini, Greece. Geosphere 2, 253–268.
Reck, H., 1936. Santorini. Der Werdergang eines Inselvulkans und sein Ausbruch 1925.Dietrich Reimer, Berlin 1928 (3 vol.).
Sakellariou, D., Sigurdsson, H., Alexandri, M., Carey, S., Rousakis, G., Nomikou, P., Georgiou, P., Ballas, D., 2010. Active tectonics in the Hellenic Volcanic Arc: the Columbo submarine volcanic zone. Bulletin of the Geological Society of Greece XLIII (2), 1056–1063.
Sakellariou, D., Rousakis, G., Nomikou, P., Croff Bell, K., Carey, S., Sigurdsson, H., 2012. Tsunami triggering mechanisms associated with the 17th cent. BC Minoan eruption of Thera Volcano, Greece. The 22nd International Offshore and Polar Engineering Conference, Tsunami and Safety Symposium, Rhodes, Greece, June 17–22, 2012.
Saltogianni, V., Stiros, S., 2012. Modelling of the Mogi magma source centre of the Santorini Volcano (Thera), Aegean Sea, 1994–1999, based on numerical–topological approach. Studia Geophysica et Geodaetica 56 (4), 1037–1062.
Schmidt, D.A., Burgmann, R., 2003. Time-dependent land uplift and subsidence in the Santa Clara Valley, California, from a large interferometric synthetic aperture radar data set. Journal of Geophysical Research 108 (B9), 2416. http://dx.doi.org/10.1029/2002JB002267.
Sigmundsson, F., 1995. GPS monitoring of volcanic deformation in Iceland. Proc. Intern. Workshop "New Challenges for Geodesy in Volcanoes Monitoring", June 14–16, 1993, Walferdange, Luxenburg: Tire a part des Cahiers du Centre Europeen de Geodynamique et de Seismologie, 8, pp. 293–305.
Sigurdsson, H., Carey, S., Alexandri, M., Vougioukalakis, G., Croff, K.L., Roman, C., Sakellariou, D., Anagnostou, C., Rousakis, G., Ioakim, C., Gogou, A., Ballas, D., Misaridis, T., Nomikou, P., 2006. Marine investigations of Greece's Santorini Volcanic Field. Eos 87 (34), 337–342.
Sotiropoulos, P., Galanopoulos, D., Lagios, E., Dawes, G.J.K., 1996. An audio-magnetotelluric (AMT) survey on Santorini Volcano, Greece. Proc. 2nd Workshop on European Laboratory Volcanoes, May 2–4, Santorini, Greece (Publ. Europ. Comm. DGXII Environment and Climate Res. Progr.), pp. 281–295.
Stiros, S., Chassapis, A., 2003. Geodetic monitoring of the Santorini (Thera) Volcano. Survey Review 37, 84–88.
Stiros, S., Psimoulis, P., Vougioukalakis, G., Fytikas, M., 2010. Geodetic evidence and modeling of a slow, small-scale inflation episode in the Thera (Santorini) Volcano caldera, Aegean Sea. Tectonophysics 494 (3–4), 180–190.
Wen, Y., Li, Z., Xu, C., Ryder, I., Brgmann, R., 2012. Post-seismic motion after the 2001 Mw = 7.8 Kokoxili earthquake in Tibet observed by InSAR time series. Journal of Geophysical Research B: Solid Earth 117 (8) (art. no. B08405).
Werner, C., Wegmuller, U., Wiesmann, A., Strozzi, T., Sensing, G., Muri, S., 2003. Interferometric point target analysis with JERS-1L-band SAR data. Proc. IGARSS, Toulouse, France, Jul. 21–25, pp. 4359–4361.
Zebker, H.A., Shanker, A.P., Hooper, A., 2007. InSAR remote sensing over decorrelating terrains: persistent scattering methods. Proc. IEEE Radar Conf, pp. 717–722.